Technical Report No. 210

036040-6-T

PRELIMINARY REPORT ON THE COOLEY-BIFI EXPERIMENT

by

Richard M. Heitmeyer
Peter W. Wood

Approved by: Theodore G. Birdsall
Theodore G. Birdsall

COOLEY ELECTRONICS LABORATORY

Department of Electrical and Computer Engineering
The University of Michigan
Ann Arbor, Michigan

for

Contract No. N00014-67-A-0181-0032
Office of Naval Research
Department of the Navy
Arlington, Virginia 22217

October 1971

ABSTRACT

An underwater acoustic propagation experiment was jointly conducted by NUSC at New London, Connecticut and a team from Cooley Electronics Laboratory at The University of Michigan. A special pseudo-random waveform, complement phase modulating a carrier was transmitted continuously for 58.5 hours. The power and angle of the carrier, the power in the sidebands, and the noise power in the signal bandwidth were recorded continuously during this time. In addition, the total power and the power spectrum in a narrow band about the carrier were recorded as a measure of the forward scattering reverberation. Also, the cross-correlation of the received signal with a stored reference was continuously computed in order to examine the multipath structure and its stability. This report presents a brief description of the experiment and the on-line analysis of the results.

ACKNOWLEDGEMENTS

The work described in this report is the result of cooperative research conducted jointly by The University of Michigan and the U. S. Navy. Signal processing was performed by the Stochastic Signal Processing Group of Cooley Electronics Laboratory (CEL), University of Michigan under the direction of Dr. T. G. Birdsall. Activities of this group are sponsored by Code 468 of the Office of Naval Research. The BIFI range is operated by Code 2211, Ocean Sciences Division of the New London Laboratory, Naval Underwater Systems Center (NUSC/NLL) under the direction of Mr. W. R. Schumacher. The data were taken as a part of the continuing shallow water research program being conducted by NUSC/NLL supported by NAVSHIPS OOV1L Exploratory Development program. The authors wish to acknowledge the work of many individuals in both groups whose enthusiastic support made successful completion of this test possible.

The most significant single task encountered in preparing for the test was the writing, testing and documentation of the real-time computer program used for data acquisition and analysis. The overall chore fell to Kurt Metzger of CEL with several major program segments being provided by Dr. Birdsall.

The signal processing scheme employed requires high-stability reference oscillators at the transmitting and receiving locations. The oscillators and associated synthesizers were provided by NUSC and were adjusted and tested over an extensive period by Mr. Hans Arens of E-71, Federal German Republic, an exchange engineer presently working at NUSC/NLL. His skill and care resulted in frequency stability which was a full order of magnitude better than had been anticipated.

The coordinator of the joint test for NUSC was Mr. Bernard Sussman. His untiring efforts and knowledge of the facilities were crucial factors in successfully dealing with problems as they arose.

Many others played an important part in preparations for, and conduct of, the test. Among these are Brian Barton of CEL who prepared materials for the test, Mrs. Ann Fulmer who assisted in documentation of programs and who has typed this report and Messrs. Carl Milner and Pete Trask of NUSC who monitored the transmitting equipment at Block Island. Messrs. Hector Bernier and Hans Arens of NUSC cooperated in the data taking phase.

TABLE OF CONTENTS

LIST OF ILLUSTRATIONS

LIST OF ILLUSTRATIONS (Cont.)

LIST OF SYMBOLS

C	carrier power measurement
S	sideband power measurement
N	noise power measurement
$\hat{S}$	actual received sideband power
$\hat{N}$	the noise power passed through the sideband processing filter
$(\hat{S}/\hat{N})$	the sideband signal-to-noise ratio
f_c	carrier frequency
D	number of cycles of carrier per digit of the modulating sequence
d	duration of the modulating sequence digit
L	number of digits in the modulating sequence
T	period of the transmitted signal
Δf	the frequency separation between the lines in the spectrum of the transmitted signal
B	frequency spread under the main lobe of the power spectrum of the transmitted signal
B_m	the tooth bandwidth in the digital processing filters
B_r	the bandwidth of the reverberation processing filter

CHAPTER I

THE COOLEY BIFI EXPERIMENT

An underwater acoustic propagation experiment was jointly conducted by NUSC at New London and a team from the Cooley Electronics Lab at The University of Michigan at Ann Arbor. This experiment is an extension of project MIMI propagation and signal processing research.

During the week of 7 September 1970 approximately 58.5 hours of reception were taken and analyzed on-line at the BIFI range of NUSC. The analysis was performed by Mr. Peter Wood and Dr. Richard Heitmeyer using the Cooley Measurement Package in the MIMI Field-8 data acquisition and signal processing equipment. In addition to the on-line analysis, about 1.5 million digital words of reception at intermediate stages of processing were recorded for later processing at CEL.

This report presents a brief description of the BIFI range, the experiment, and some of the on-line analysis. A more complete report is planned.

I.1 The BIFI Range

The material in this section is taken from Ref. 1. A more complete discussion on the BIFI range can be found there.

Location and Facilities

The BIFI range, illustrated in Fig. 1, is part of the New London Laboratory of the Naval Underwater System Center located at New London, Connecticut. It extends from Block Island (BI), Rhode Island to Fisher Island (FI), New York, a distance of 18.6 nautical miles, and to Watch Hill Point, Rhode Island, a distance of 12 nautical miles. The Cooley-BIFI experiment used only the BI to FI portion of the range.

The transmitting site for the BIFI range is located on Block Island. Bottom mounted, omnidirectional projectors are located at point S (Fig. 1) and connected to BI by cable. The projectors used were a 400 Hz Minneapolis-Honeywell source with a bandwidth of 70 Hz and a source level of 89 dB/1 μbar/1 yard, and a 127 Hz Minneapolis-Honeywell source with a bandwidth of 25 Hz and a source level of 106 dB/1 μbar/1 yard.

The receiving site used for the experiment is located at Fisher Island. A bottom-mounted DT-5S hydrophone located at point H_1 in Fig. 1, and connected to FI by submarine cable, was used for the experiment. This phone was approximately three feet off the bottom at a depth of 150 feet.

Both the transmitting site and the receiving site are connected to the BIFI laboratory at NUSC by telephone lines. A telephone line to the transmitter site at BI was used in the experiment to provide

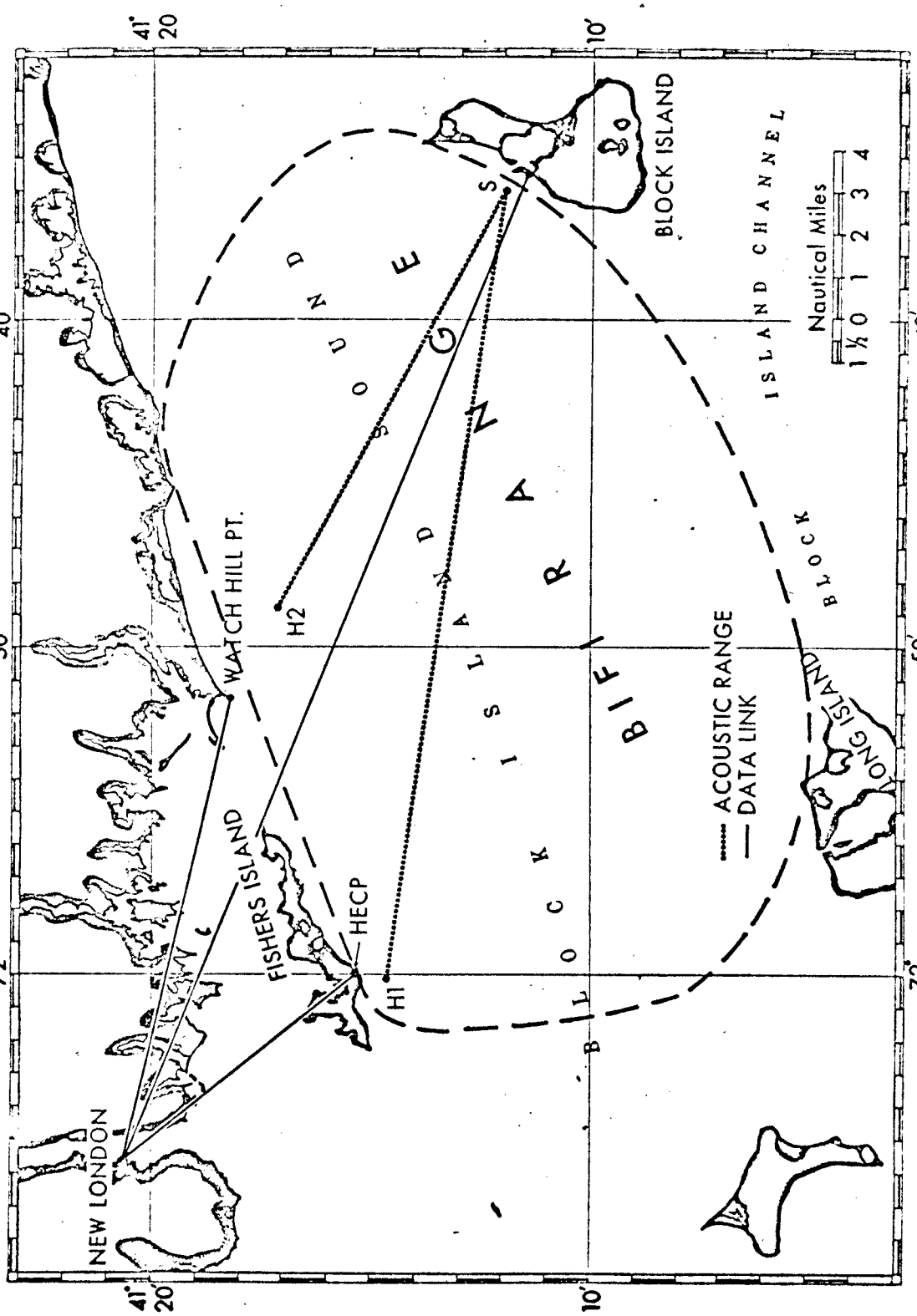

Source: USL Tech Memo 2211-281-68

Fig. 1. BIFI range

voice communications between BI and the BIFI lab at NUSC. To transmit the received signal from the hydrophones at FI back to the BIFI lab for processing, a 15 kHz B.W. telephone line was used.

Oceanographic and Acoustical Characteristics

The BIFI range is a shallow water range. From BI, the water depth drops to 110 feet in about one mile. It stays at that depth for approximately 10 miles and then becomes irregular over the remaining distance to FI. The composition of the bottom is soft mud and sand from BI, becoming progressively more rocky as FI is approached. The bottom profile is shown in Fig. 2.

The general character of the velocity gradient for the BIFI range depends on the season. In summer, the velocity gradient is negative resulting in mostly bottom reflecting paths. In winter the velocity gradient is slightly positive and the paths become mostly surface reflecting. Iso-velocity contours for both summer and winter are shown in Fig. 3. Summer conditions were presumed to hold for this experiment.

Previous work by NUSC predicted the propagation loss in September at the frequencies of interest would be approximately 90 dB at 127 Hz and 110 dB at 400 Hz.

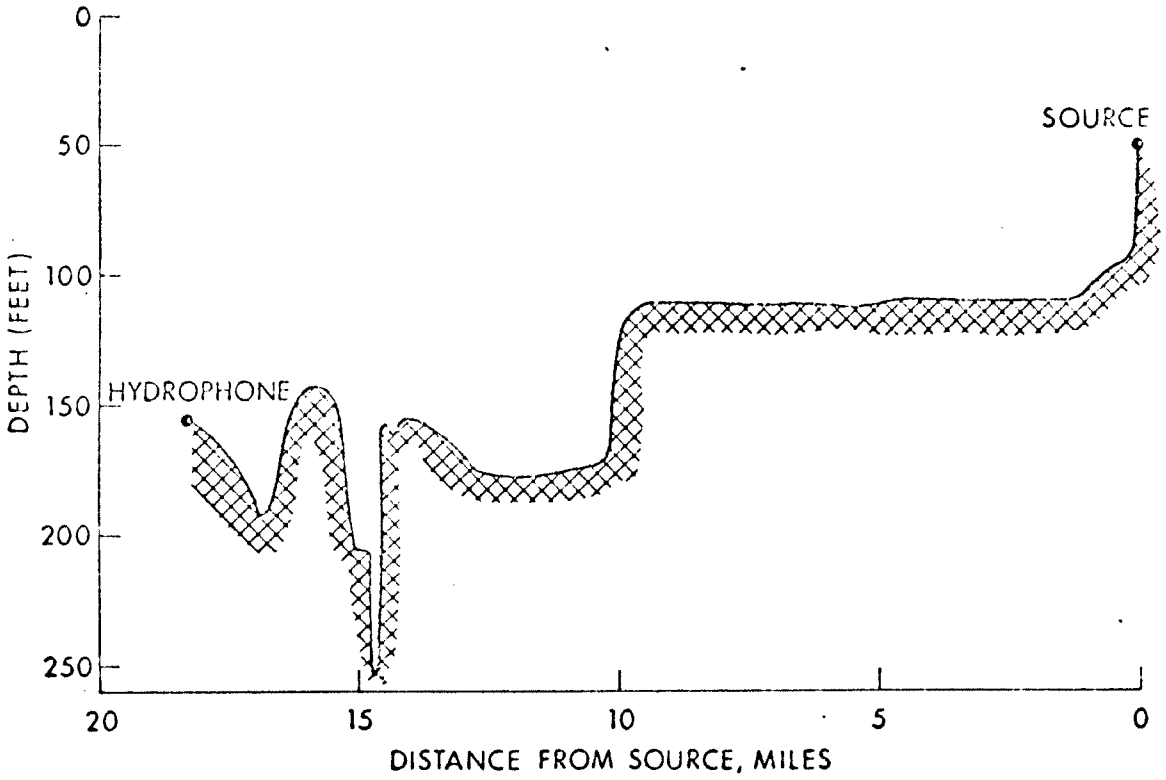

Source: USL Tech Memo 2211-281-68

Fig. 2. Bottom profile, Block Island to Fishers Island

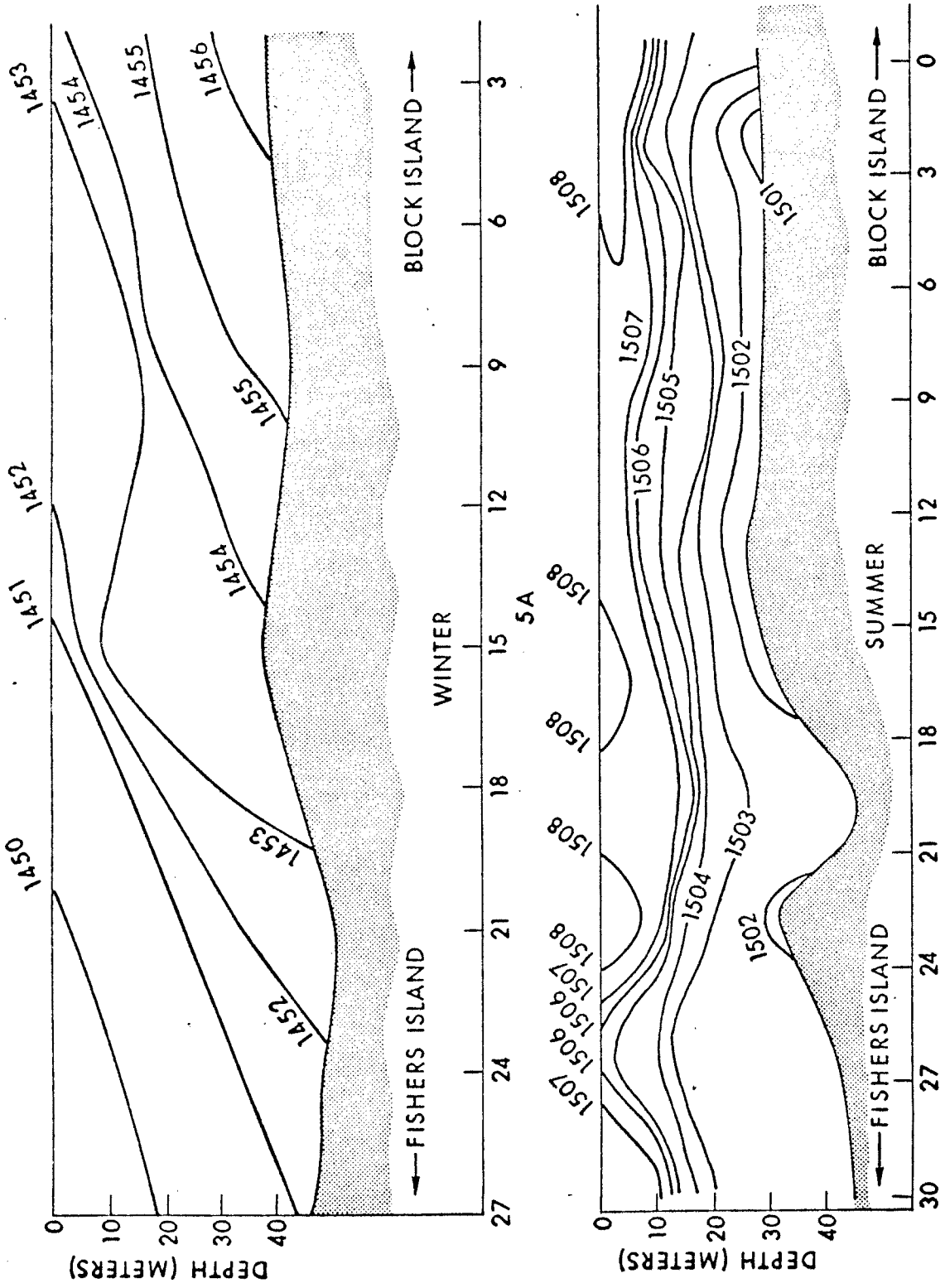

Source: USL Tech Memo 2211-281-68

Fig. 3. Sound velocity contours (M/S) block island sound

I.2 The Transmitted Signals

Two different signals were used for the Cooley-BIFI experiment. Each of these signals consisted of a linear-maximal binary sequence, complement-phase modulating a carrier. The phase of the carrier is either $+45^{o}$ or -45^{o} depending on the value of the binary digit in the modulating sequence. A portion of such a waveform is shown in Fig. 4 where:

f_c carrier frequency

d duration of the sequence digit

D number of cycles of carrier per sequence digit.

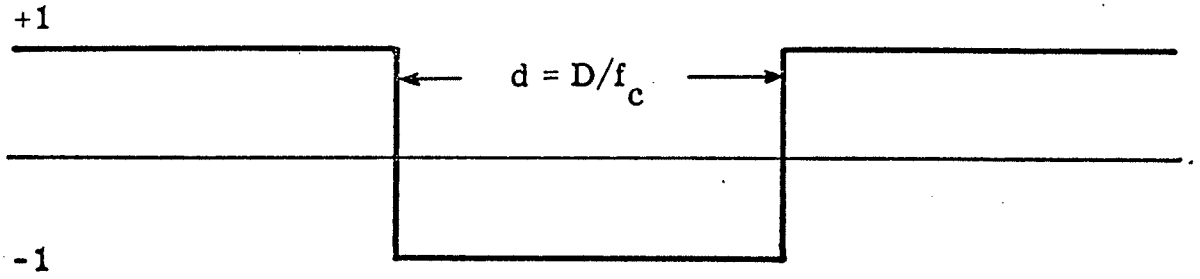

(a)

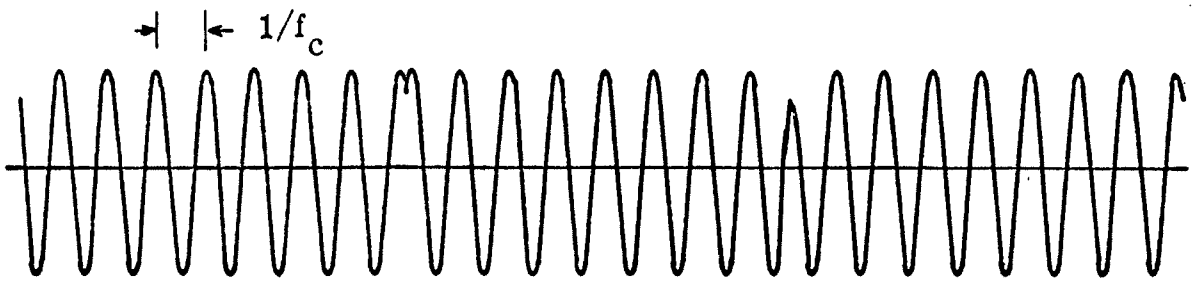

(b)

Fig. 4. A complement-phase modulated signal
(a) a portion of the modulating waveform
(b) the resulting transmission

Both of the signals used in the experiment had an integral number of cycles per digit D. The signals are periodic with period T given by

$$T = L\,d = LD/f_c$$

where L is the number of digits in one period of the modulating sequence. For the two signals of interest in this experiment

$f_c = 400$ Hz

$D = 8$

$d = 0.02$ sec

$L = 31$

$T = 0.62$

and

$f_c = 127$ Hz

$D = 8$

$d = 0.063$ sec

$L = 15$

$T = 0.945$

The bandwidth, B, (frequency spread under the main lobe) and the spectral line spacing, Δf, for the two signals are (see Fig. 5).

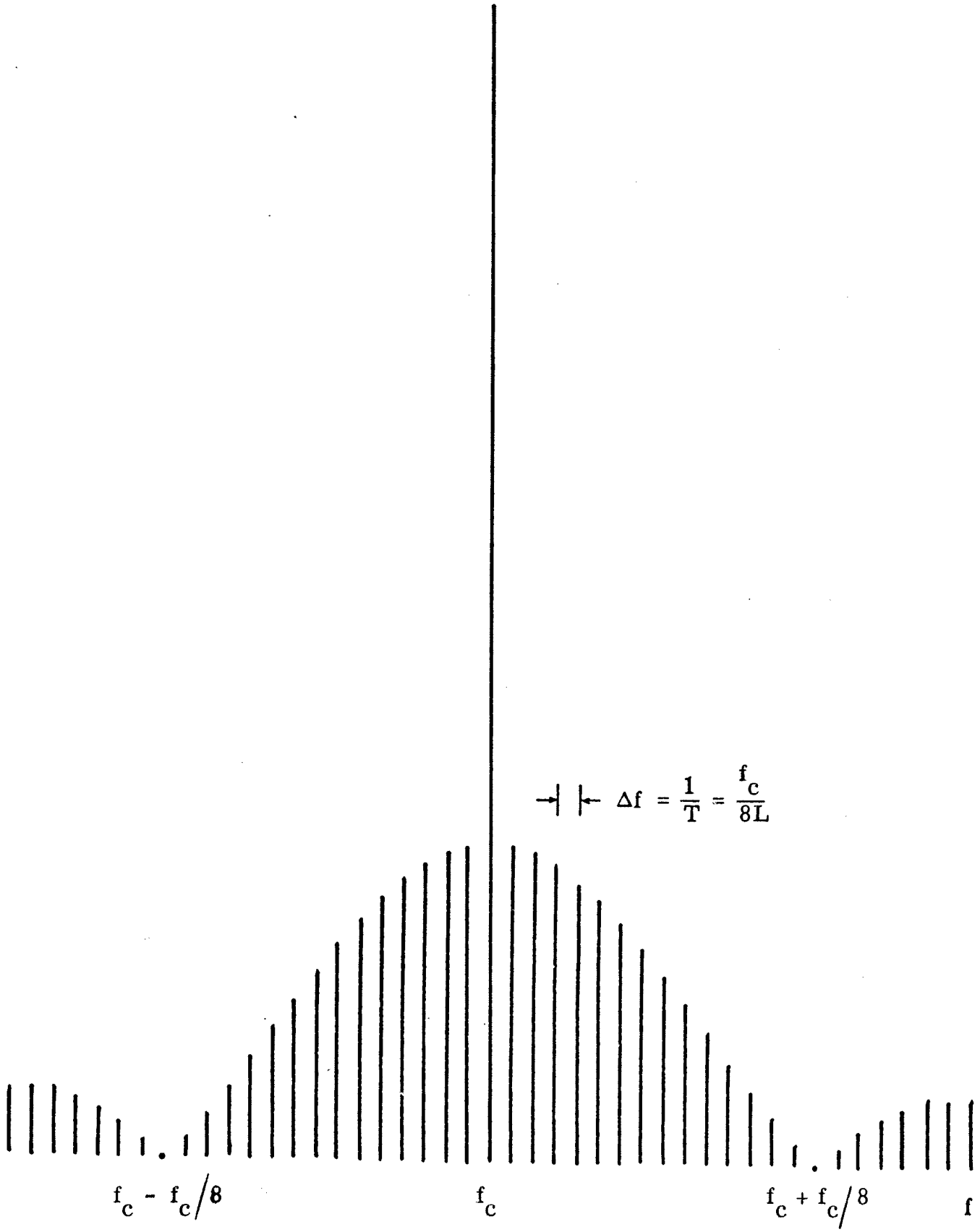

Fig. 5. The RMS spectrum of a complement-phase modulated signal for L = 15 , D = 8

for the 400 Hz signal

$$B = 100 \text{ Hz} \qquad \Delta f = 1.61 \text{ Hz}$$

and for the 127 Hz signal

$$B = 32 \text{ Hz} \qquad \Delta f = 1.06 \text{ Hz}$$

The number of spectral lines between the first two zeros is $2L-1$, and the fraction of the total power in the carrier is

$$\frac{1}{2}\left(1 + \frac{1}{L^2}\right) \approx \frac{1}{2}$$

I.3 The Equipment Configuration

The configuration of the equipment used in the Cooley-BIFI experiment is shown in Fig. 6. The signal generating equipment at the transmitting site, and the signal processing equipment at the receiving site were provided by Cooley; the source, hydrophones and frequency references were supplied by NUSC. Stability of the frequency reference was investigated by H. J. Arens and reported in Ref. 2. Both references are more stable than 1 part in 10^9.

The different components in Fig. 6 function as follows. The output of the frequency synthesizer at the transmitting site is a sine wave at a frequency equal to $4 \times f_c$. This signal is converted to a square wave reference, at the same frequency, by the phase-locked function generator. The resulting square wave is then used as a clock

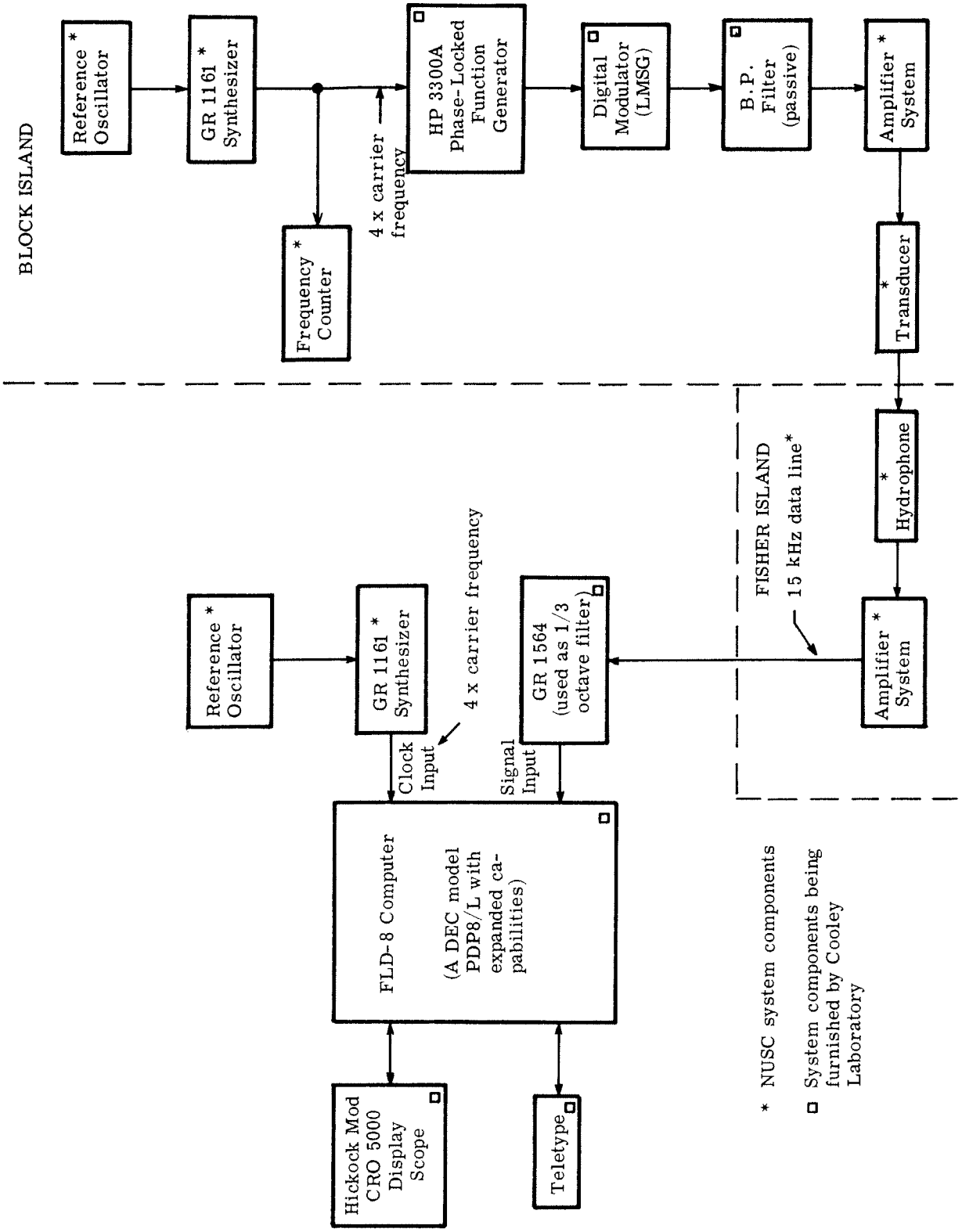

Fig. 6. The Cooley-BIFI experiment equipment configuration

to the digital modulator whose output, after filtering, is the signal described in the preceding section. This signal is amplified and then transmitted down the BIFI range. It is received at Fisher Island and sent over phone lines to the NUSC lab. At the lab it is first filtered with a 1/3 octave filter and then processed by the FIELD-8 computer.

I.4 Quantities Measured

The measurements made in the Cooley-BIFI experiment fall into one of three categories: (1) power and angle measurements of the received signal, (2) measurements of the surface reverberation effect, and (3) measurements of the multipath arrivals. Each set of measurements is computed and recorded every 100 seconds. For the 400 Hz signal, each set of measurements is computed on the basis of approximately 80 seconds of data and for the 127 Hz signal each set of measurements is computed on the basis of approximately 60 seconds of data.

I.4.1 Power and Angle Measurements.

C Power. The C power measurement is a measure of the power present in the carrier of the received signal transmission. It is determined as that power passed through a digital processing filter with a frequency response as illustrated in Fig. 7a. The bandwidth of this filter, B_m, depends on the signal transmitted. In particular

B_m = 0.013 Hz for the 400 Hz transmission

and

B_m = 0.016 Hz for the 127 Hz transmission.

N Power. The N power measurement is a measure of the noise power contained within the main lobe of the received signal spectrum: $f_c - B/2 \leq |f| \leq f_c + B/2$. It is determined as that power passed through the digital processing filter with a frequency response as illustrated in Fig. 7c. Such a filter is often referred to as a comb filter. It is to be noted that each tooth in the comb filter of Fig. 7c is centered midway between the spectral lines in the signal spectrum. Moreover, the bandwidth of each tooth is B_m, the same B_m as used for the carrier power measurement.

S Power. The S power measurement is a measure of the signal power within the main lobe of the received signal power spectrum, excluding the carrier power. It is determined as that power passed through the digital processing filter of Fig. 7b. This filter is recognized as a comb filter with a tooth missing at the carrier frequency. The remaining teeth are aligned with the line frequencies of the transmitted signal. The bandwidth of each tooth is also B_m.

Sideband Signal-to-Noise Ratio $\hat{S}/\hat{N}$. The sideband signal-to-noise ratio is a measure of the signal-to-noise ratio of the output of the

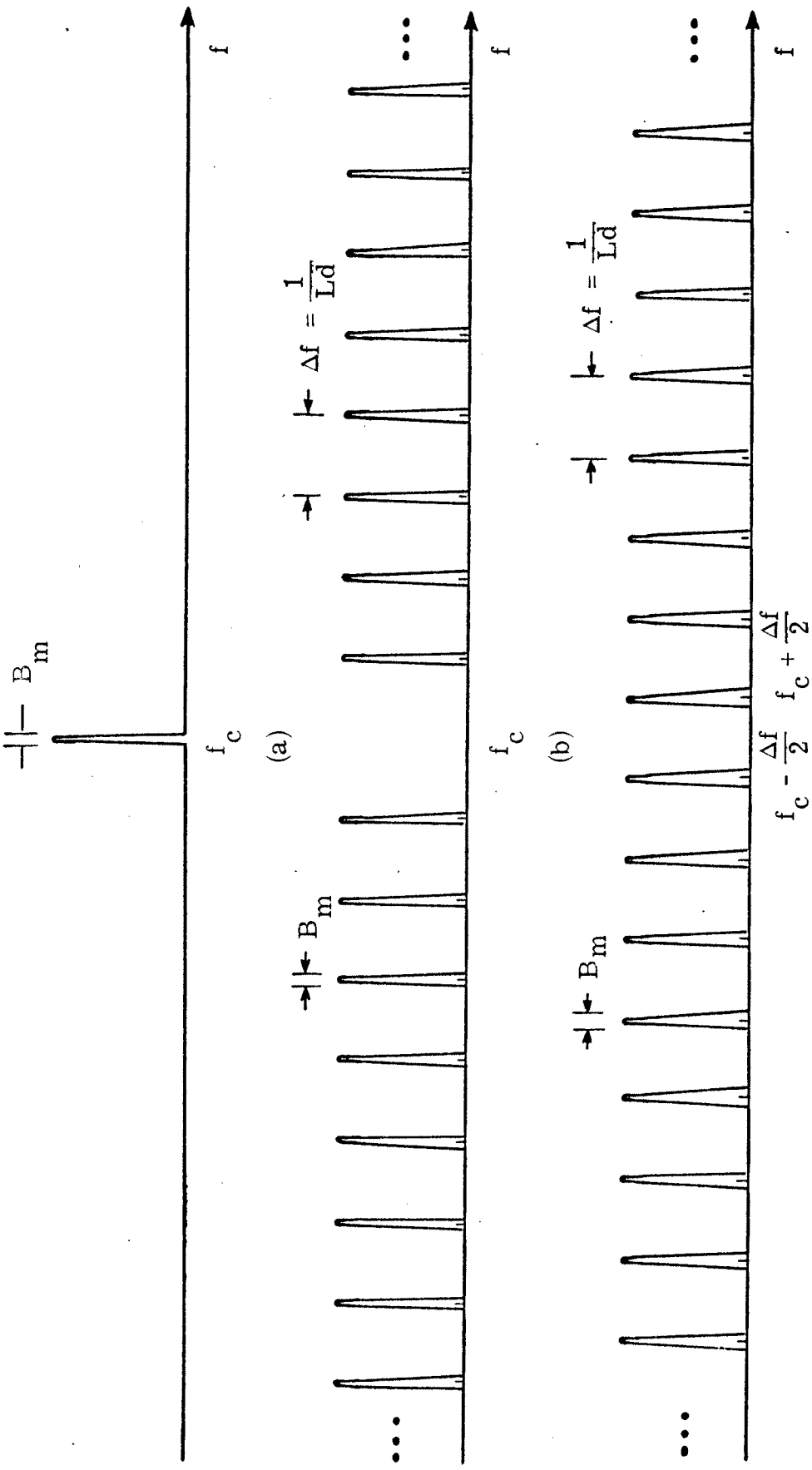

Fig. 7. The frequency response of the digital processing filters
(a) carrier power filter, (b) sideband power filter,
(c) noise power filter

sideband processing filter of Fig. 7b. This quantity is not measured directly, although it can be related to the measurements as follows.

Denote the actual sideband power at the output of the sideband processing filter by $\hat{S}$ watts and denote the actual noise power at the output of the sideband processing filter by $\hat{N}$ watts. Let the noise power out of the noise processing filter be denoted by $\tilde{N}$. Then

$$S = 10 \log_{10} (\hat{S} + \hat{N}) \tag{1}$$

and

$$N = 10 \log_{10} (\tilde{N}) \tag{2}$$

so that

$$S - N = 10 \log_{10} \left(\frac{\hat{S}}{\tilde{N}} + \frac{\hat{N}}{\hat{N}} \right)$$

Except for statistical fluctuations and the effect of one missing tooth in the sideband processing filter, $\hat{N}$ and $\tilde{N}$ are equal. Therefore

$$S - N \cong 10 \log_{10} \left(\frac{\hat{S}}{\hat{N}} + 1 \right) \tag{3}$$

The output sideband signal-to-noise ratio, $\hat{S}/\hat{N}$, is inferred from S - N using (3) whenever $S > N$. The input sideband signal-to-noise ratio is 20.8 dB below this for the 400 Hz signal and 18.1 dB below for the 127 Hz signal.

Carrier Angle (A). The carrier angle is a measure of the relative difference between the phase of the output of the carrier processing filter (Fig. 7a) and the phase of the local reference oscillator (Fig. 6).

I.4.2 Surface Reverberation Measurements. The effect of surface reverberation is to scatter some of the power of a transmitted frequency into sidebands on either side of that frequency. It is felt that this scattered power should lie between 0.1 Hz and 0.4 Hz on either side of the transmitted frequency, depending upon the spectrum of the surface waves. For the signals used in the Cooley-BIFI experiment, the spacing between the lines in the power spectrum is large enough so that the sideband line frequencies do not interfere with the power scattered from the carrier frequency. Thus, the surface reverberation effect can be measured by computing the power spectrum of the received signal in a bandwidth B_r centered about the carrier line. The bandwidth B_r is chosen large enough to include the power scattered by surface reverberation but small enough to exclude the power in the sideband line frequencies. In particular, B_r was taken as 0.8 Hz for the 400 Hz signal and 1.06 Hz for the 127 Hz signal. In addition to calculating the reverb power spectra, the total power in the bandwidth B_r minus the carrier power was calculated for each data set.

I.4.3 Multipath Arrival Measurements. The cross-correlation function between the demodulated received signal and a pulse-compression reference was used to measure the multipath structure of the channel. In the absence of noise, this function has a triangular peak of width, 2d, centered at the arrival time of each signal path (mod T) with an amplitude proportional to the amplitude of the signal transmitted over that path. This is the same as if a single large one-digit pulse had been transmitted once every T seconds and received through a matched filter.

As a measure of the time stability of the channel multipath structure, the zero-delay cross-correlation coefficient between the demodulated received signal and the replica was calculated for each data set. When this coefficient fell below a set value, indicating a marked change in the multipath structure, the current signal became the replica and the new multipath picture displayed. Otherwise, the previous replica and display were held. The changing magnitude of the correlation coefficient is an indicator of how fast the multipath structure is changing.

CHAPTER II

THE RESULTS OF THE ON-LINE ANALYSIS

In this chapter the results of the on-line analysis of the 58.5 hours of the Cooley-BIFI data are presented. Of the total data, 56.5 hours of data were taken using the 400 Hz signal transmission and 2 hours of data were taken using the 127 Hz transmission. During the 400 Hz signal transmission, the experiment was interrupted twice, with the result that the largest portion of uninterrupted 400 Hz measurements was 41.75 hours.

II.1 Power and Angle Measurements

This section contains plots of S-N, the three powers S, C and N and the carrier angle as continuous functions of time. (The continuity is obtained by a linear interpolation between successive data points.) The different powers appearing in these plots are expressed in decibels above an arbitrary reference and the carrier angle is expressed in terms of the number of cycles relative to the phase of the reference oscillator.

A plot of S-N and N power for the 400 Hz signal appears in Figs. 8a - 8e and the corresponding quantities for the 127 Hz signal are illustrated in Fig. 9. Both of these plots include two additional vertical scales, one for the output sideband signal-to-noise

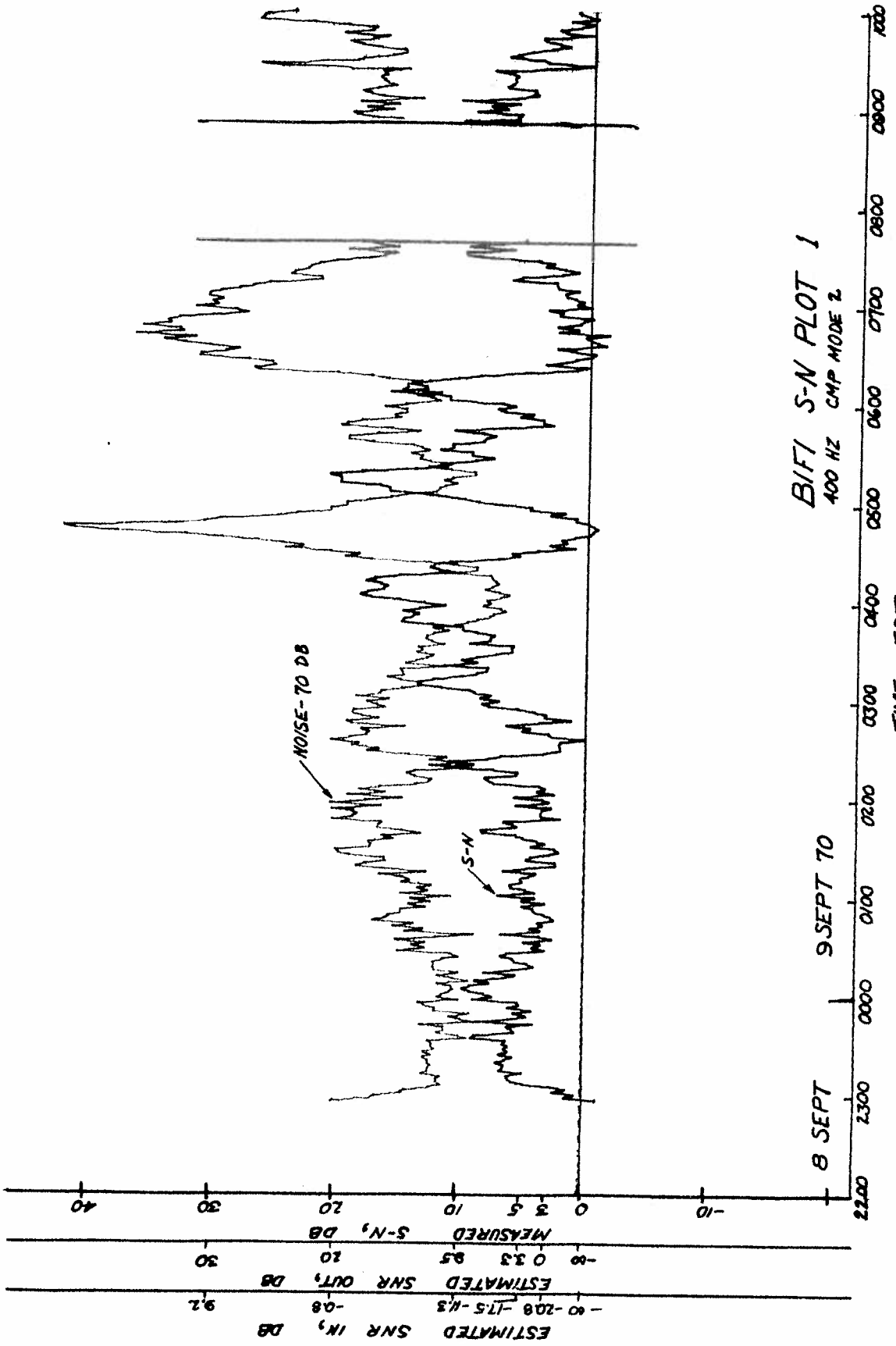

Fig. 8. Sideband signal-to-noise plot for the 400 Hz signal
(a) BIFI S-N plot 1

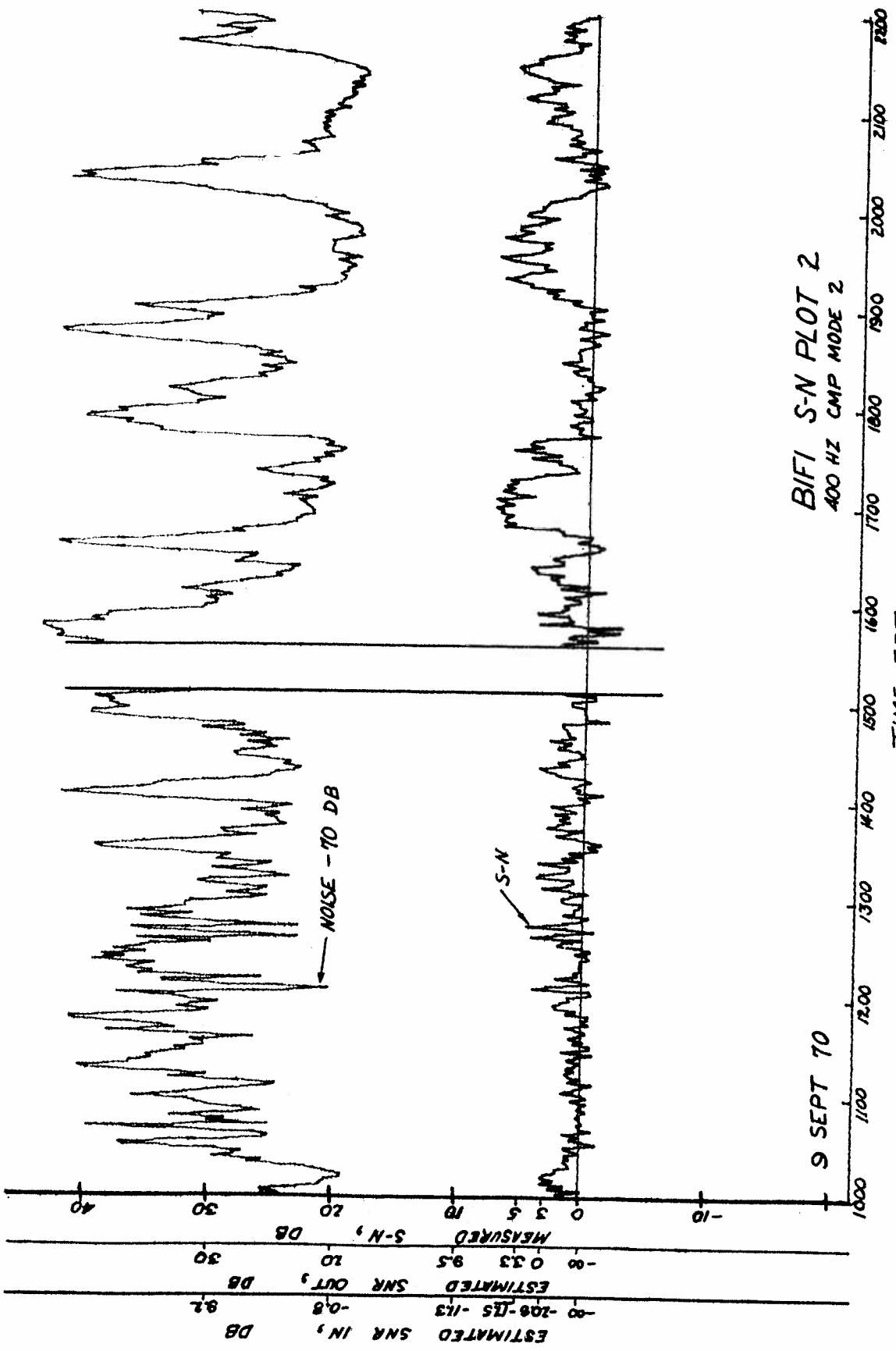

Fig. 8(b). BIFI S-N plot 2

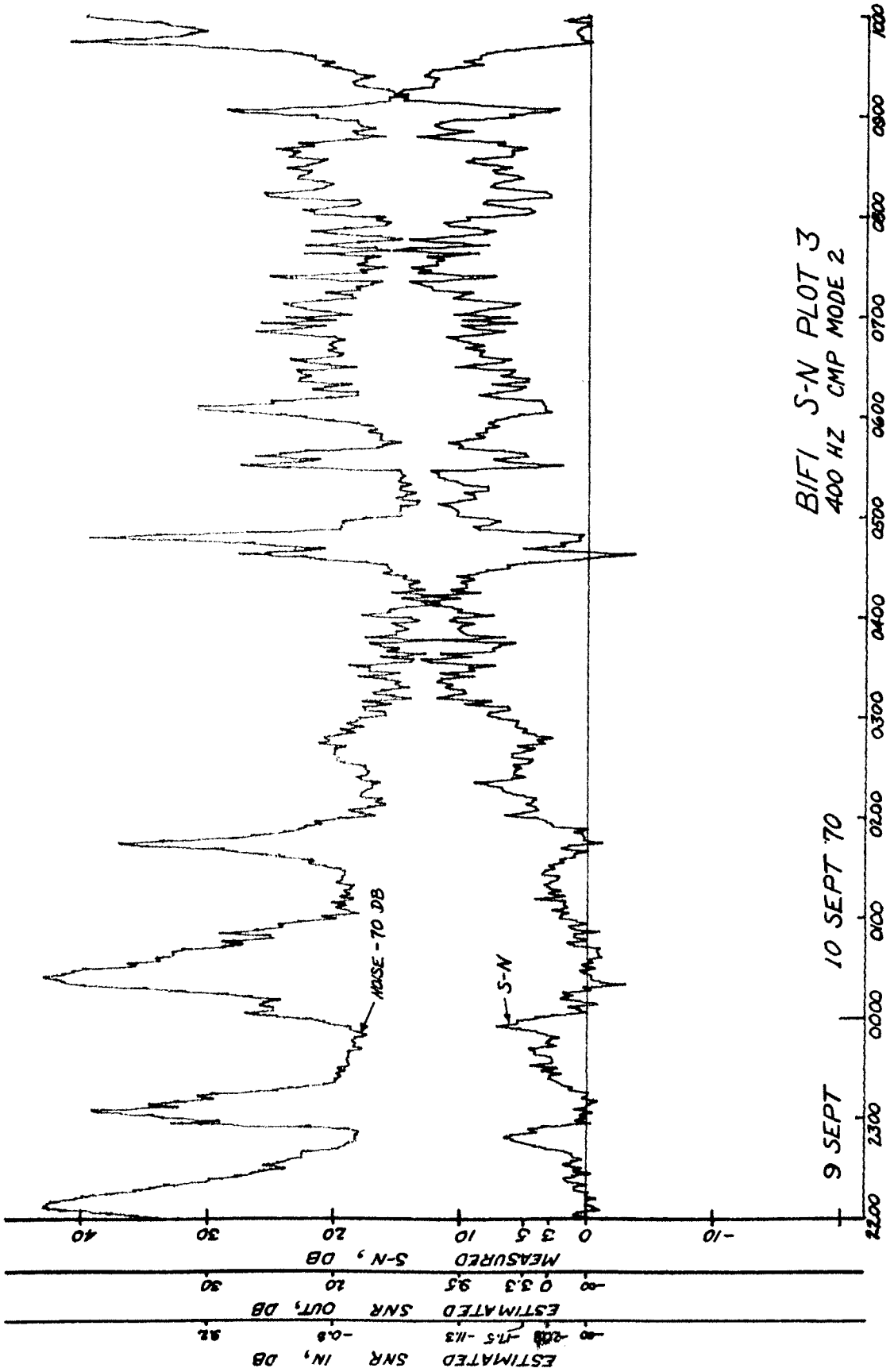

Fig. 8(c). BIFI S-N plot 3

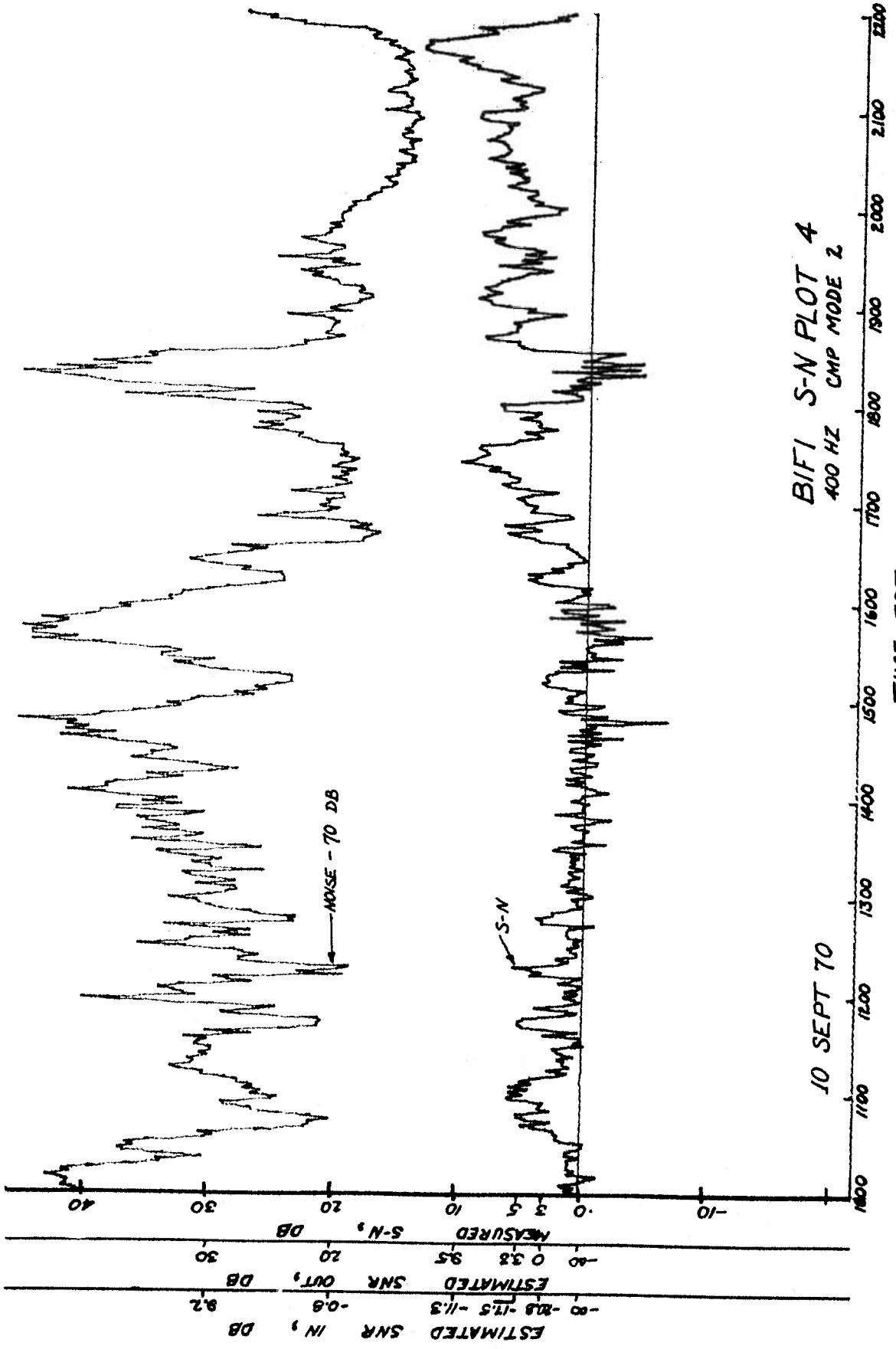

Fig. 8(d). BIFI S-N plot 4

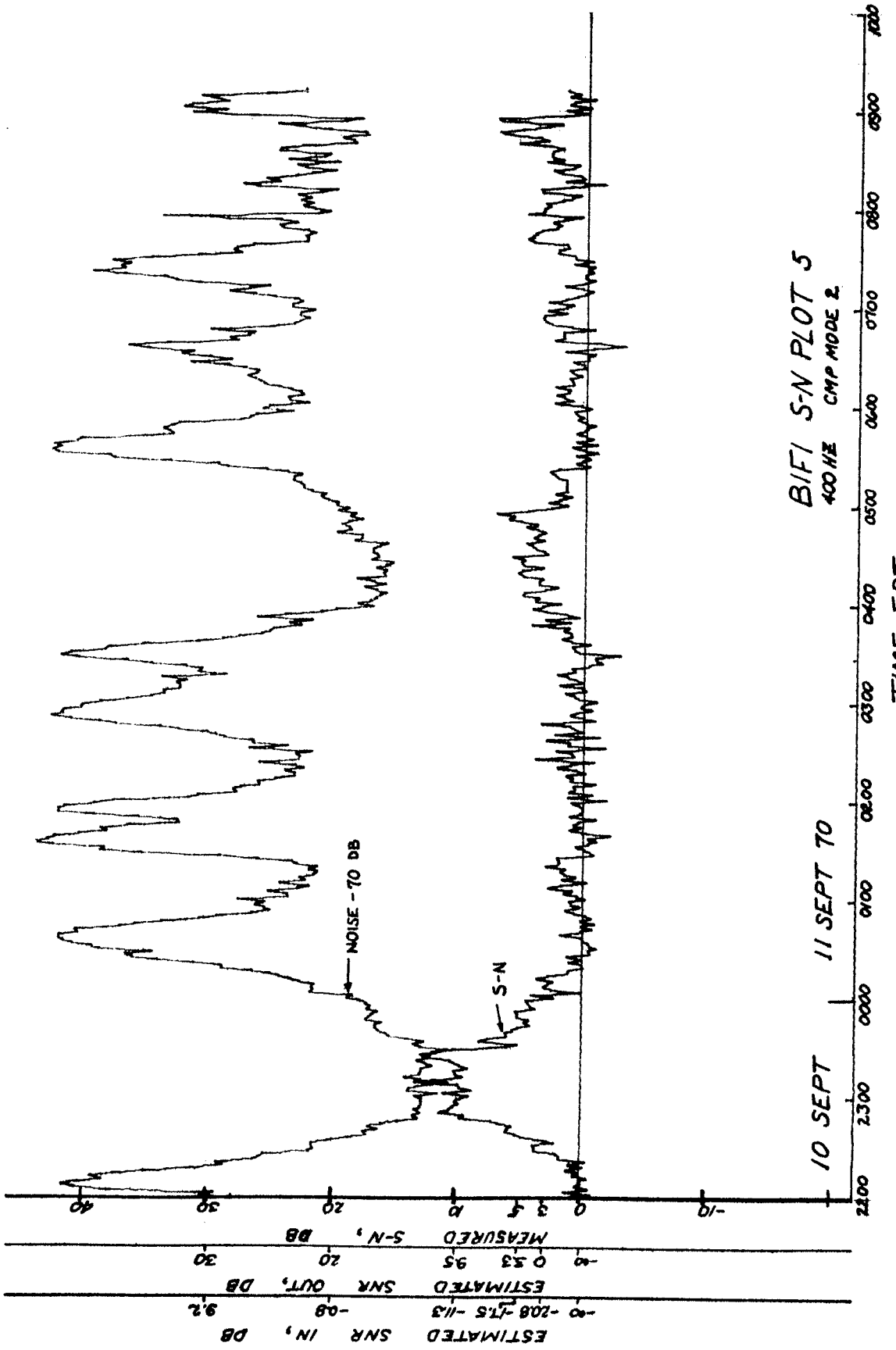

Fig. 8(e). BIFI S-N plot 5

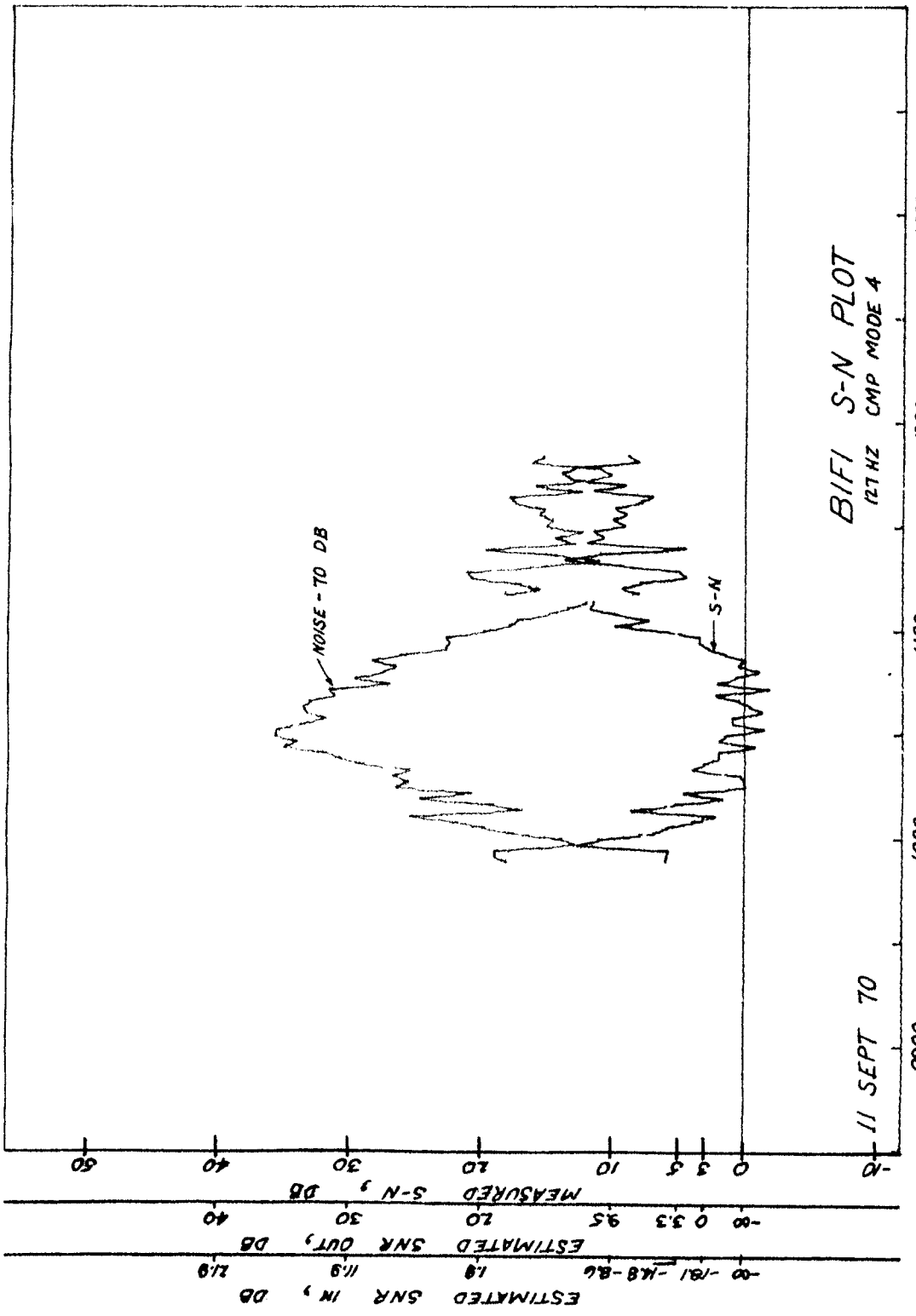

Fig. 9. Sideband signal-to-noise plot for the 127 Hz signal

ratio $\hat{S}/\hat{N}$ and one for the input sideband signal-to-noise ratio. The relation between these quantities and S - N is discussed in Section I.4.3. It is noted that key correspondences are

$$S - N = 0 \text{ dB} \longleftrightarrow \hat{S}/\hat{N} = -\infty \text{ dB}$$

$$S - N = 3 \text{ dB} \longleftrightarrow \hat{S}/\hat{N} = 0 \text{ dB}$$

and for large S/N

$$S - N \approx \hat{S}/\hat{N}$$

When the S - N measurement drops below zero, the scale relating S/N to the sideband signal-to-noise ratio $\hat{S}/\hat{N}$ is not valid.

The most important feature to be noted from Figs. 9 and 10 is that S - N only occasionally takes on values large enough to indicate a significant sideband signal component in the reception. Part of the signal degradation is due to the very large bursts of N power that occur frequently during the course of the experiment. (Most, if not all, of these bursts of N power can be attributed to the local shipping noise.) The remaining signal degradation is the result of the relatively large amount of propagation loss on the BIFI range.

Figures 10a - 10e plot S power, C power and N power for the 400 Hz signal transmission and Fig. 11 plots the same quantities for the 127 Hz transmission. These plots are referred to as the unity-gain plots since the vertical scaling is determined as if the processing filters in Figs. 7a - 7c all have gain equal to one at the peak of each tooth.

In Figs. 10 and 11 it is noted that, in general S (sideband power) is greater than or equal to N (noise power) even during the bursts of shipping noise. This is a consequence of the fact that the S measurement consists of not only the true sideband power $\hat{S}$, but also the component of noise $\hat{N}$ where

$$N \approx 10 \log_{10} \hat{N}$$

A second feature to be noted in Figs. 10 and 11 is that, unlike the S (sideband power) measurement, C (carrier power) is only slightly affected by the bursts of shipping noise. This is reasonable since the noise passed through the single tooth C power processing filter (Fig. 7a) is only a fraction of the noise passed through the S multi-tooth comb filter (Fig. 7b).

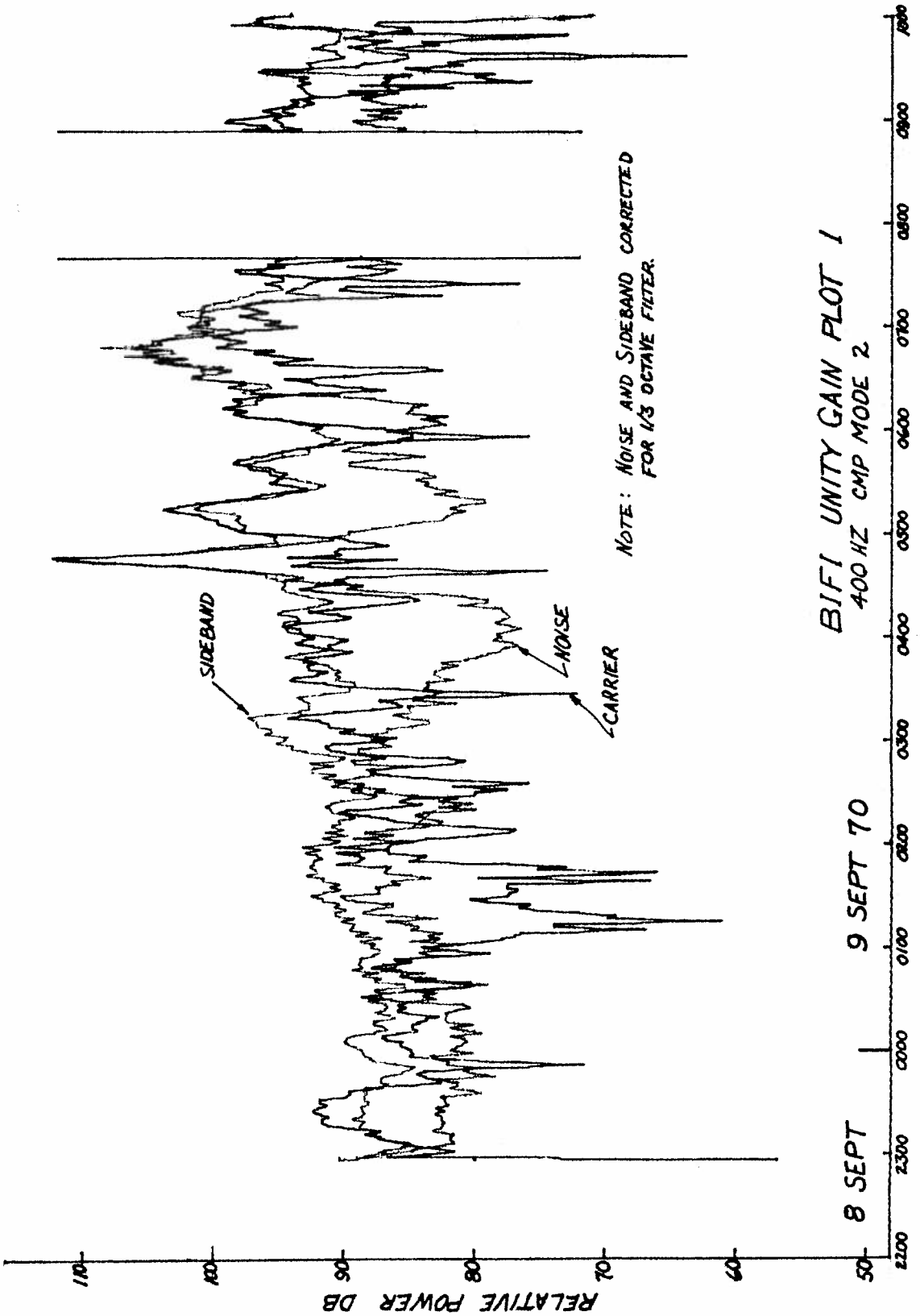

Fig. 10. Unity gain plot for the 400 Hz signal
(a) BIFI unity gain plot 1

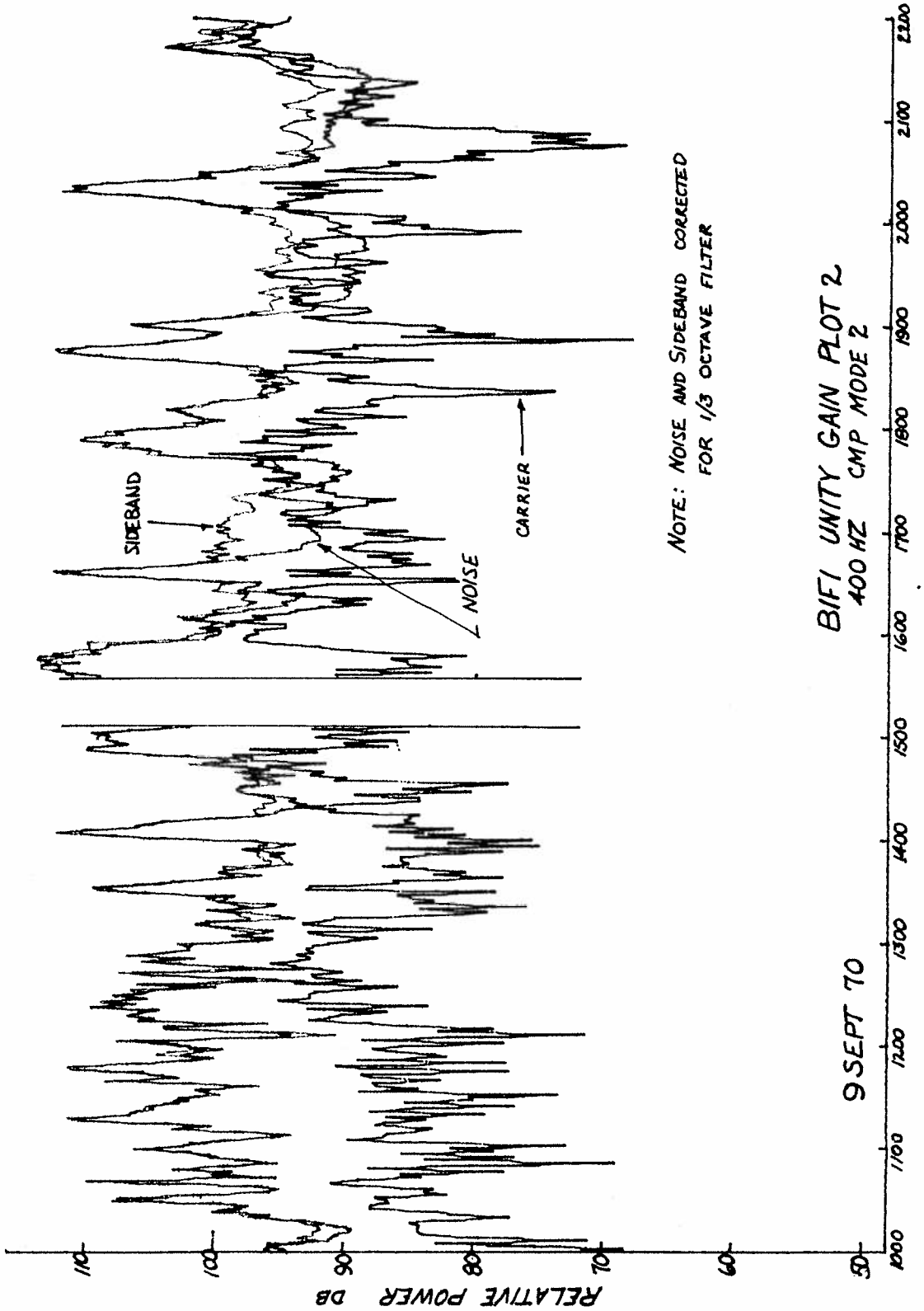

Fig. 10(b). BIFI unity gain plot 2

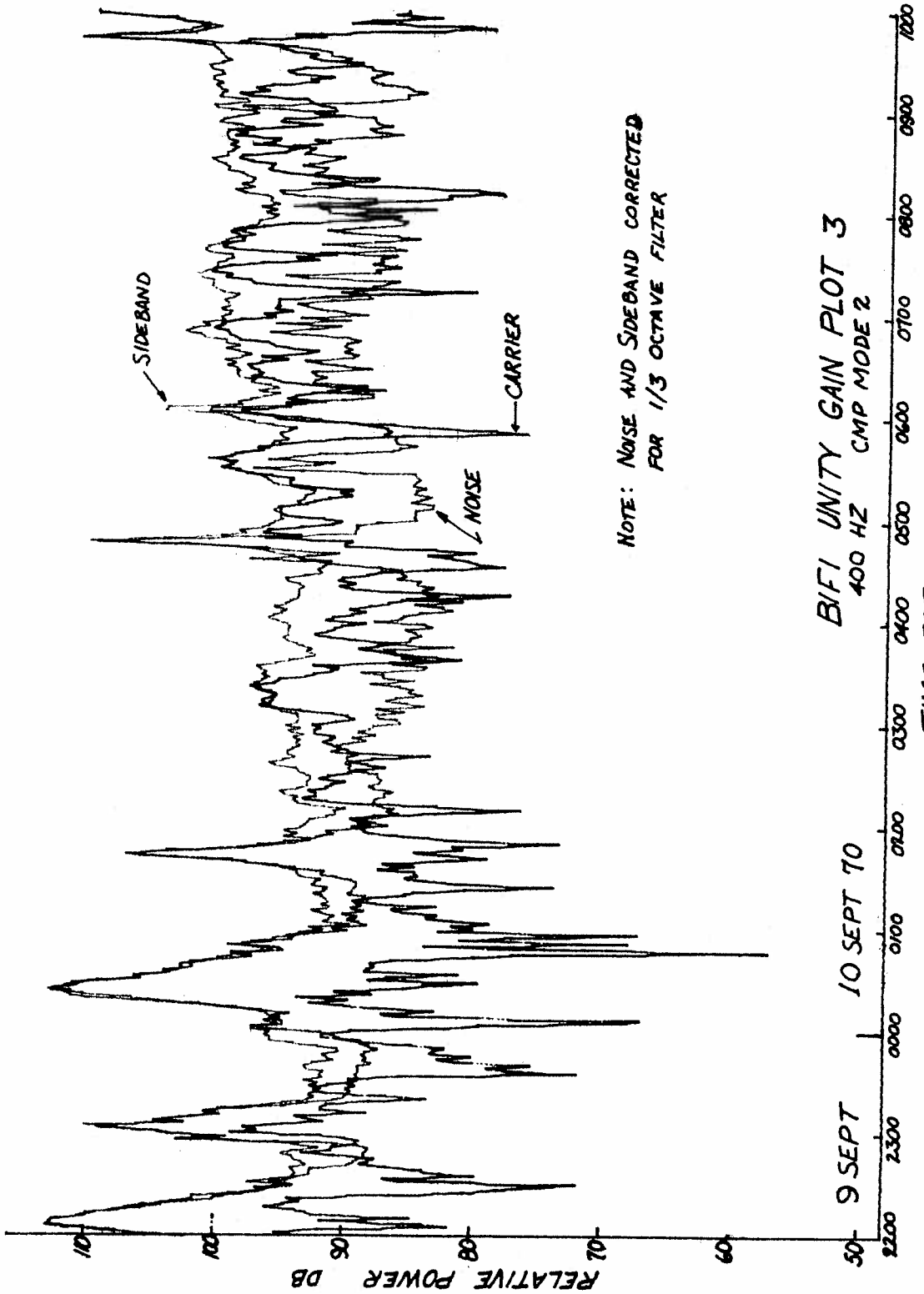

Fig. 10(c). BIFI unity gain plot 3

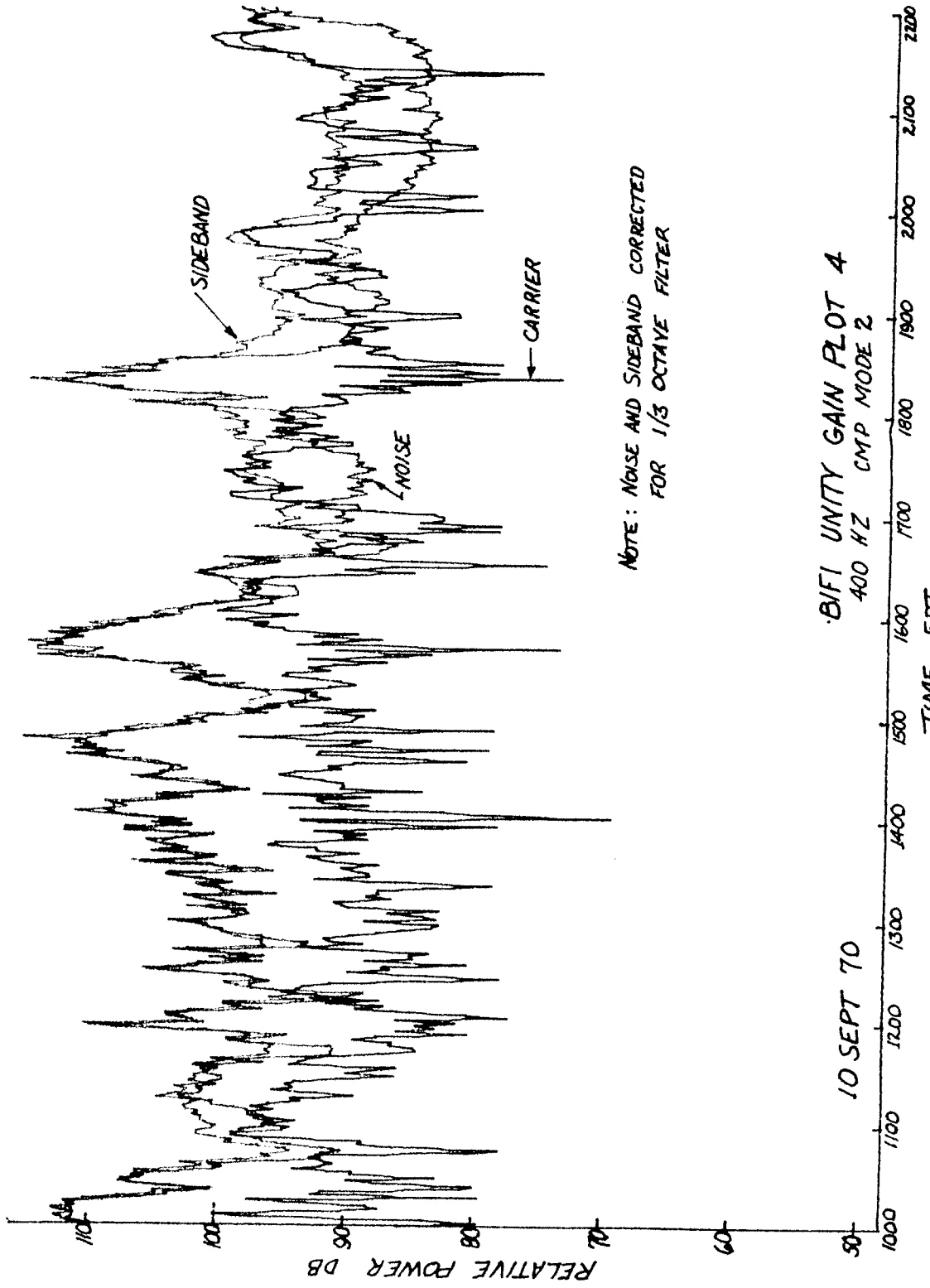

Fig. 10(d). BIFI unity gain plot 4

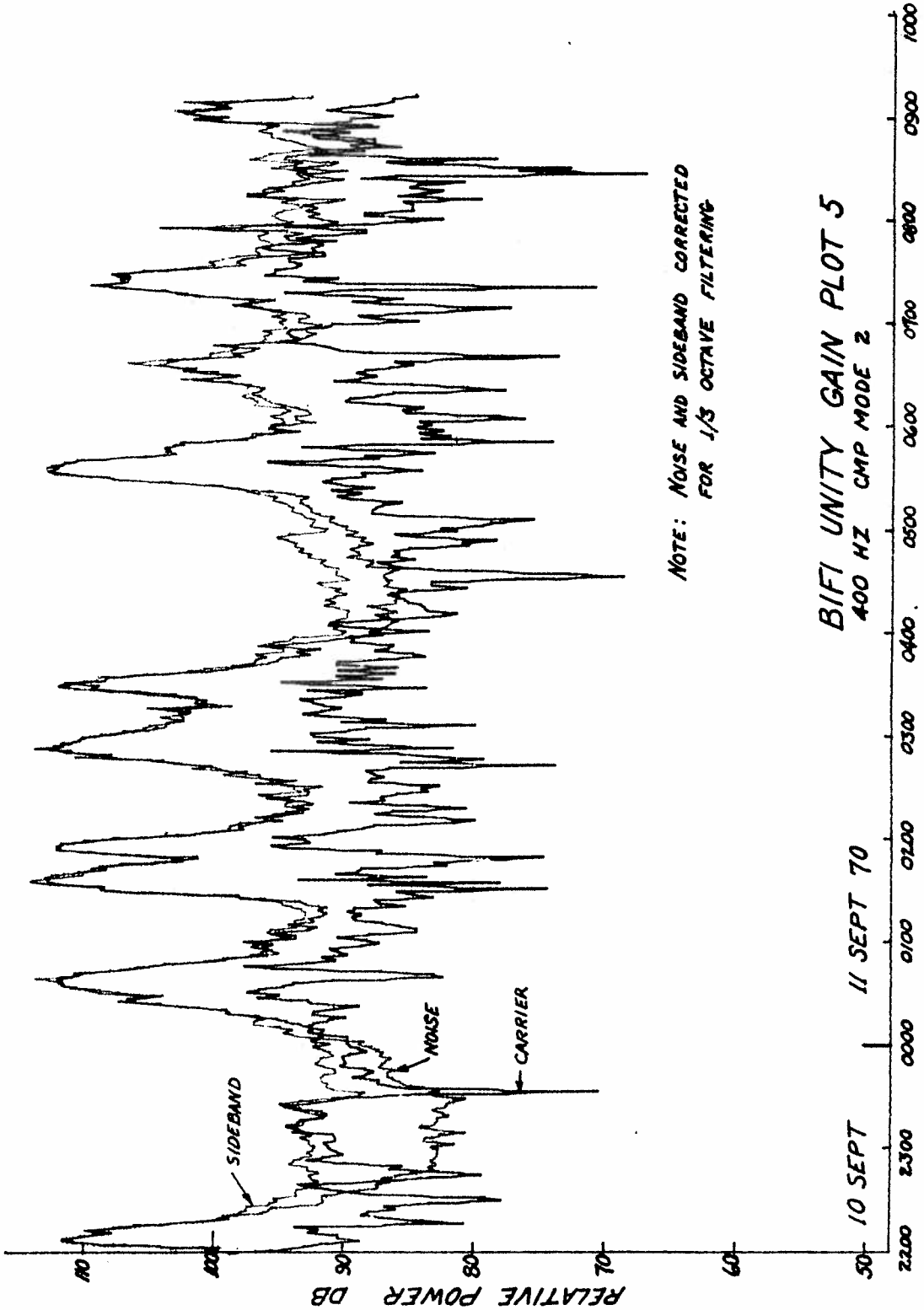

Fig. 10(e). BIFI unity gain plot 5

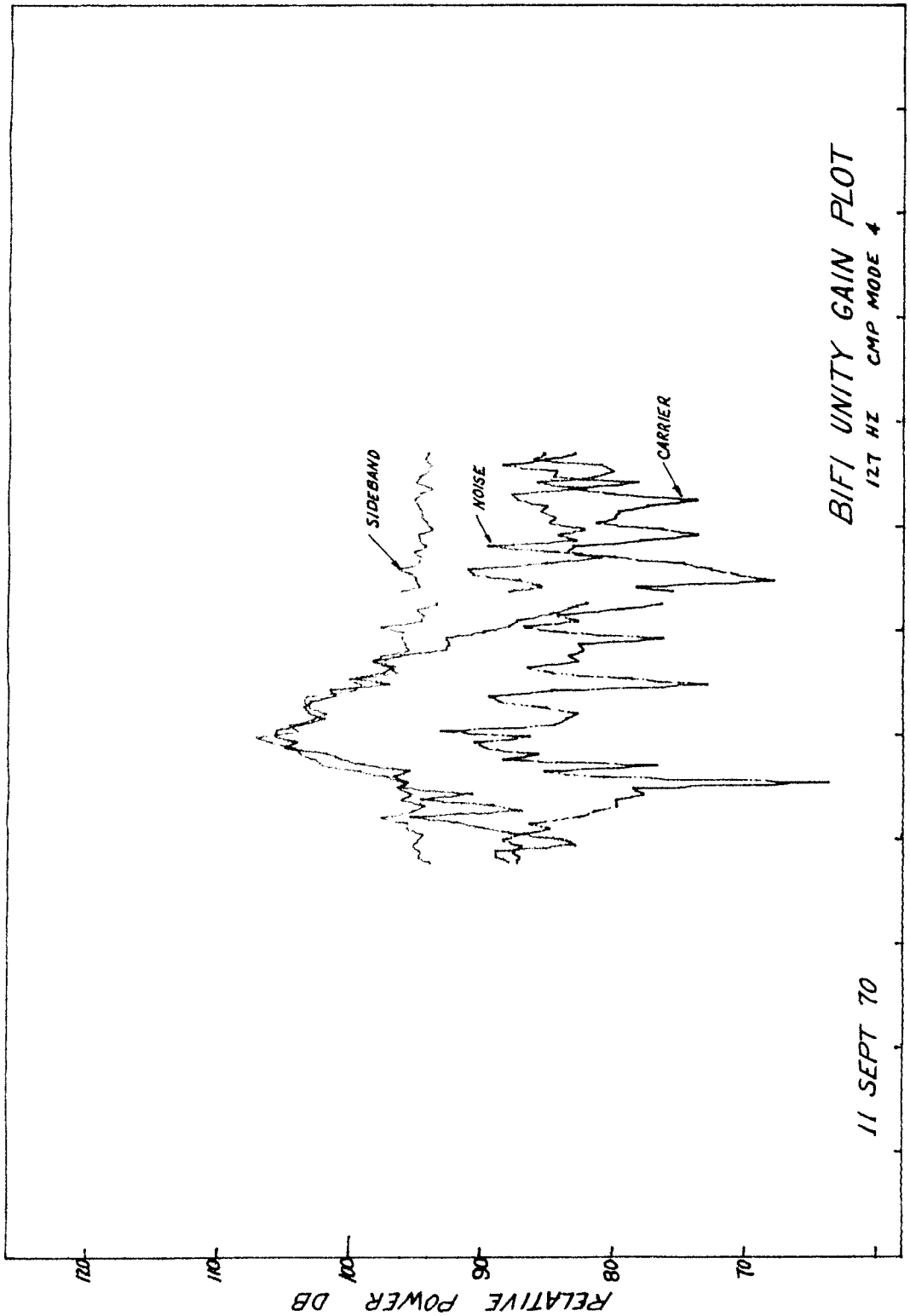

Fig. 11. Unity gain plot for the 127 Hz signal

Figures 12a - 12e and Fig. 13 again plot S power, C power and N power for the 400 Hz and 127 Hz transmission respectively. The vertical scaling on these plots, however, is determined as if the product of the power gain and the bandwidth of the processing filters of Fig. 7 is constant. This scaling is equivalent to adding a constant gain to the C power plot for both signal transmissions. This additive gain is 20.9 dB for the 400 Hz and 17.8 dB for the 127 Hz signal transmissions. The resulting plots are referred to as "constant gain-bandwidth" plots.

The constant gain-bandwidth plots are best suited for illustrating the behavior of the C power measurement. In Figs. 12 and 13 the large amount of variation in C power relative to the variation in S power is apparent. This behavior can be modeled by viewing the ocean as a time varying narrow notched filter. The C power fades occur when the notch passes through the carrier frequency line. The S power, however, remains relatively unaffected by the motion of the notch if the notch bandwidth is modeled to be only a small fraction of the total signal bandwidth.

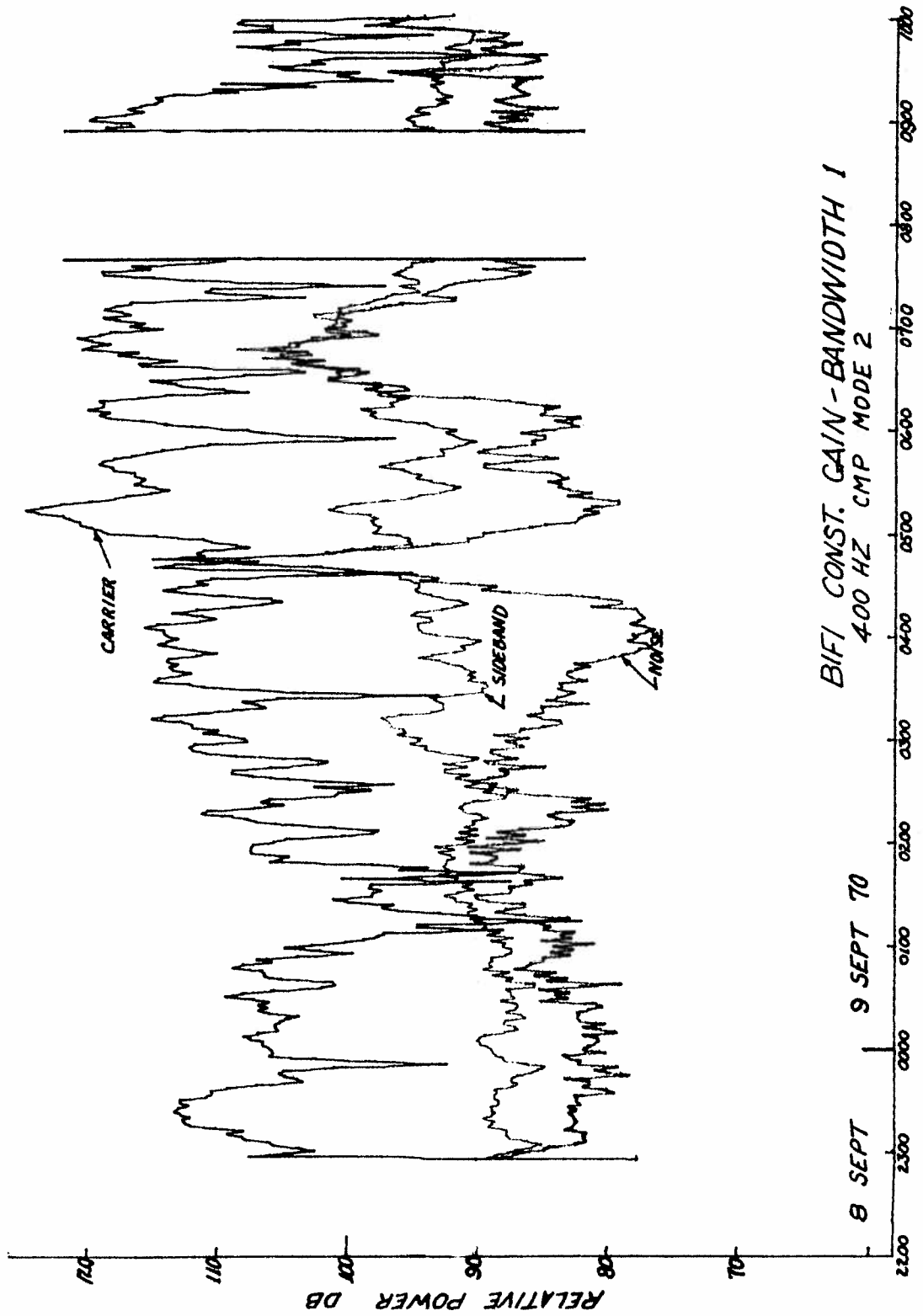

Fig. 12. Constant gain plot for the 400 Hz signal
(a) BIFI constant gain-bandwidth 1

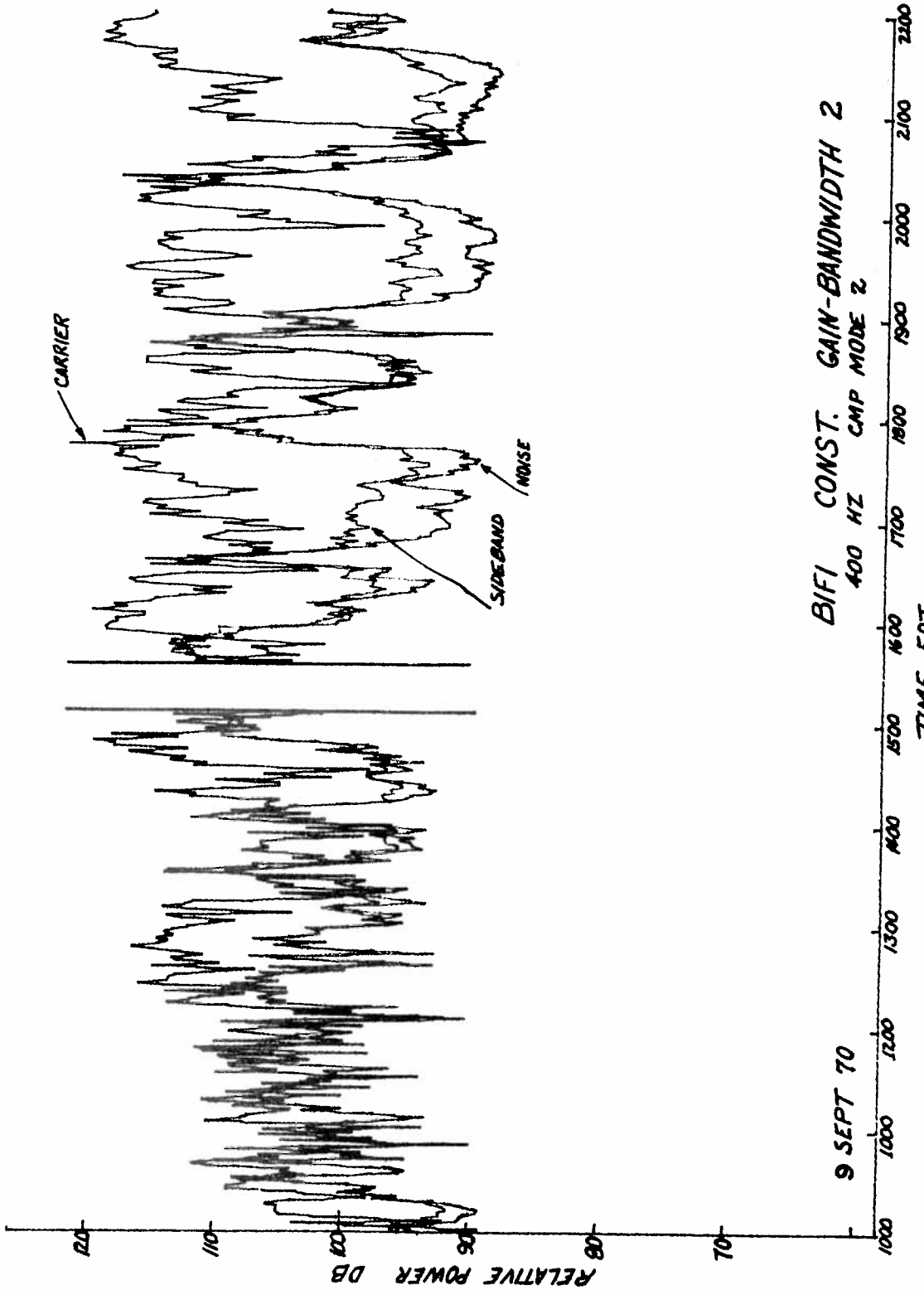

Fig. 12(b). BIFI const. gain-bandwidth 2

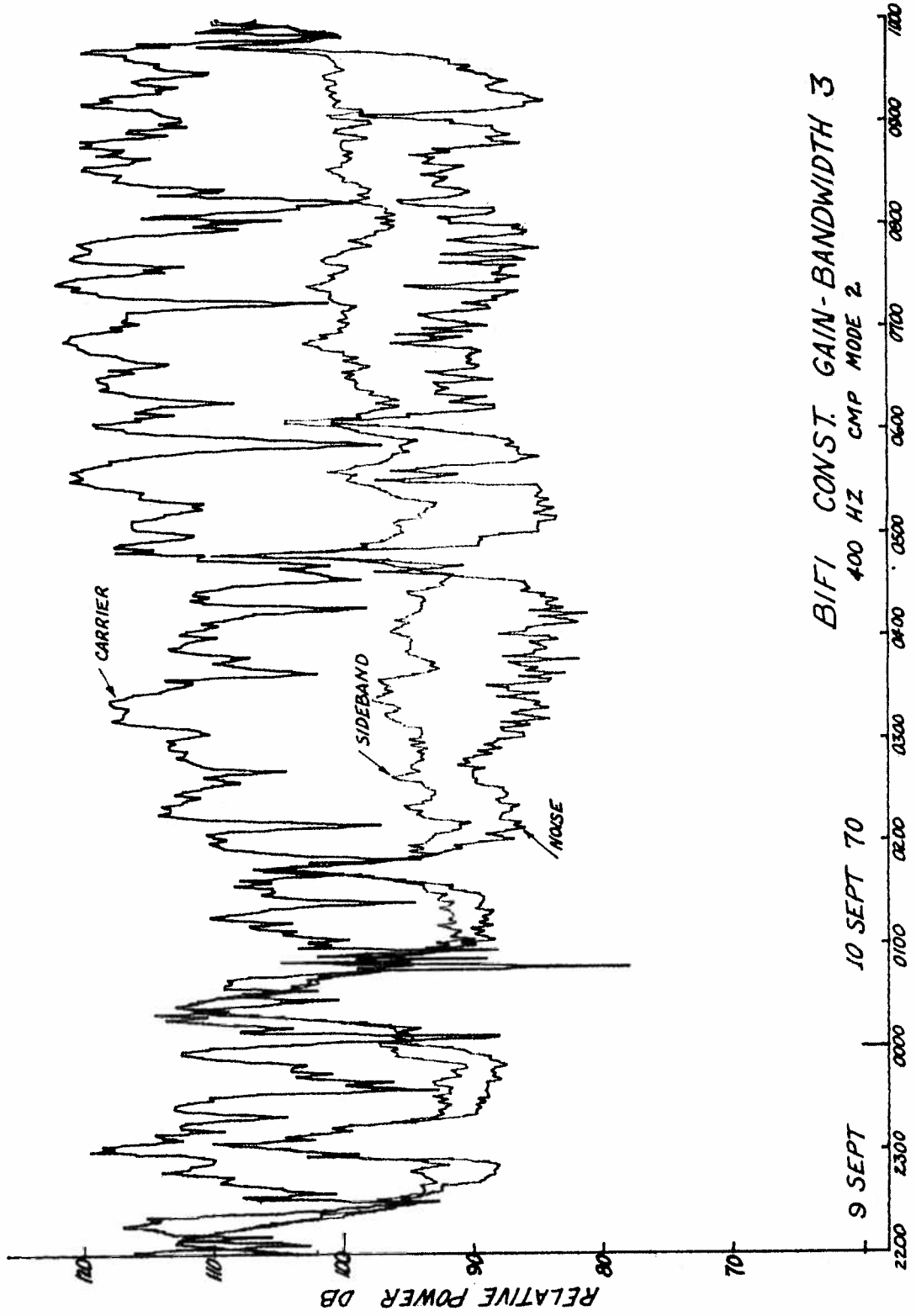

Fig. 12(c). BIFI const. gain-bandwidth 3

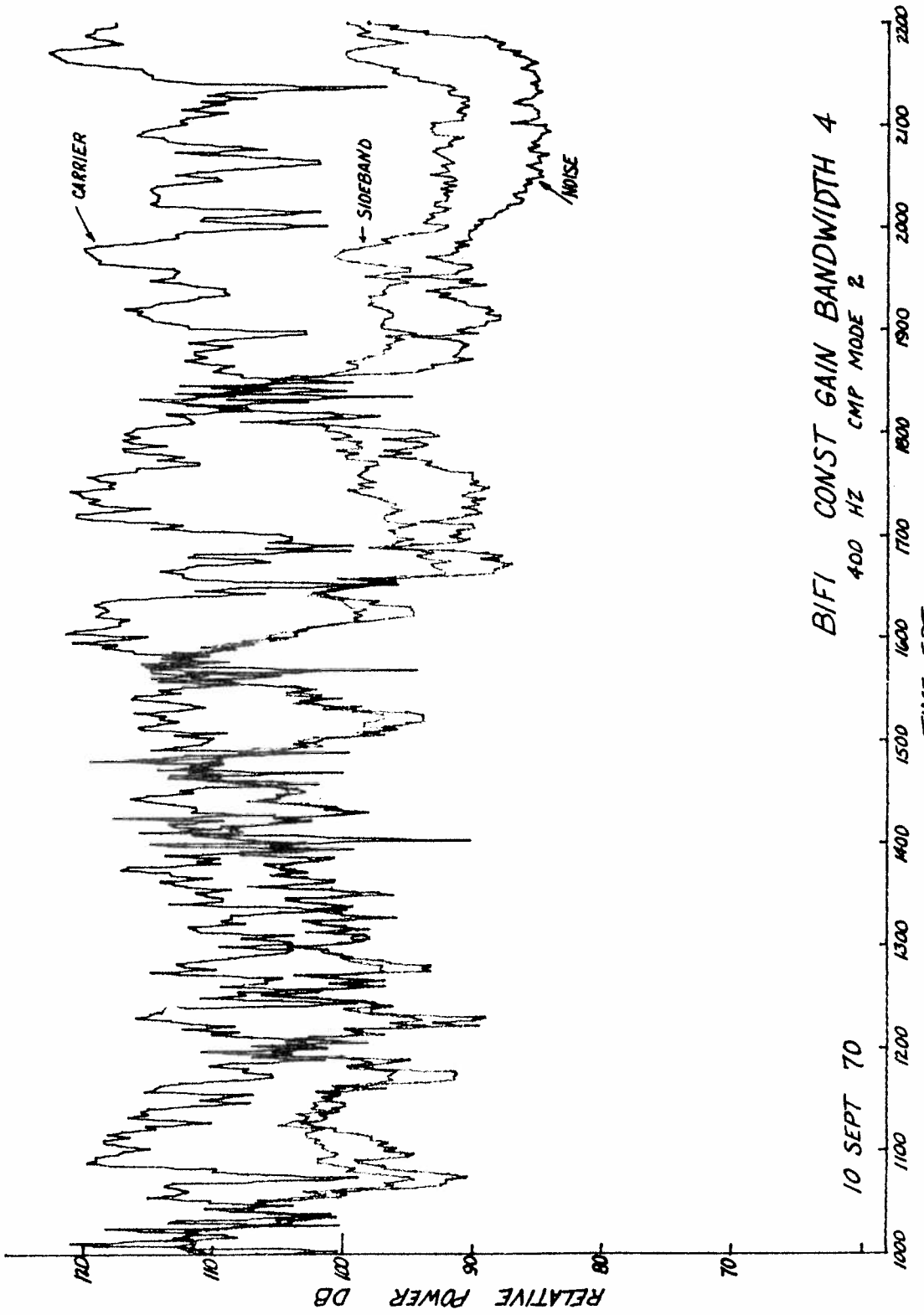

Fig. 12(d). BIFI const. gain-bandwidth 4

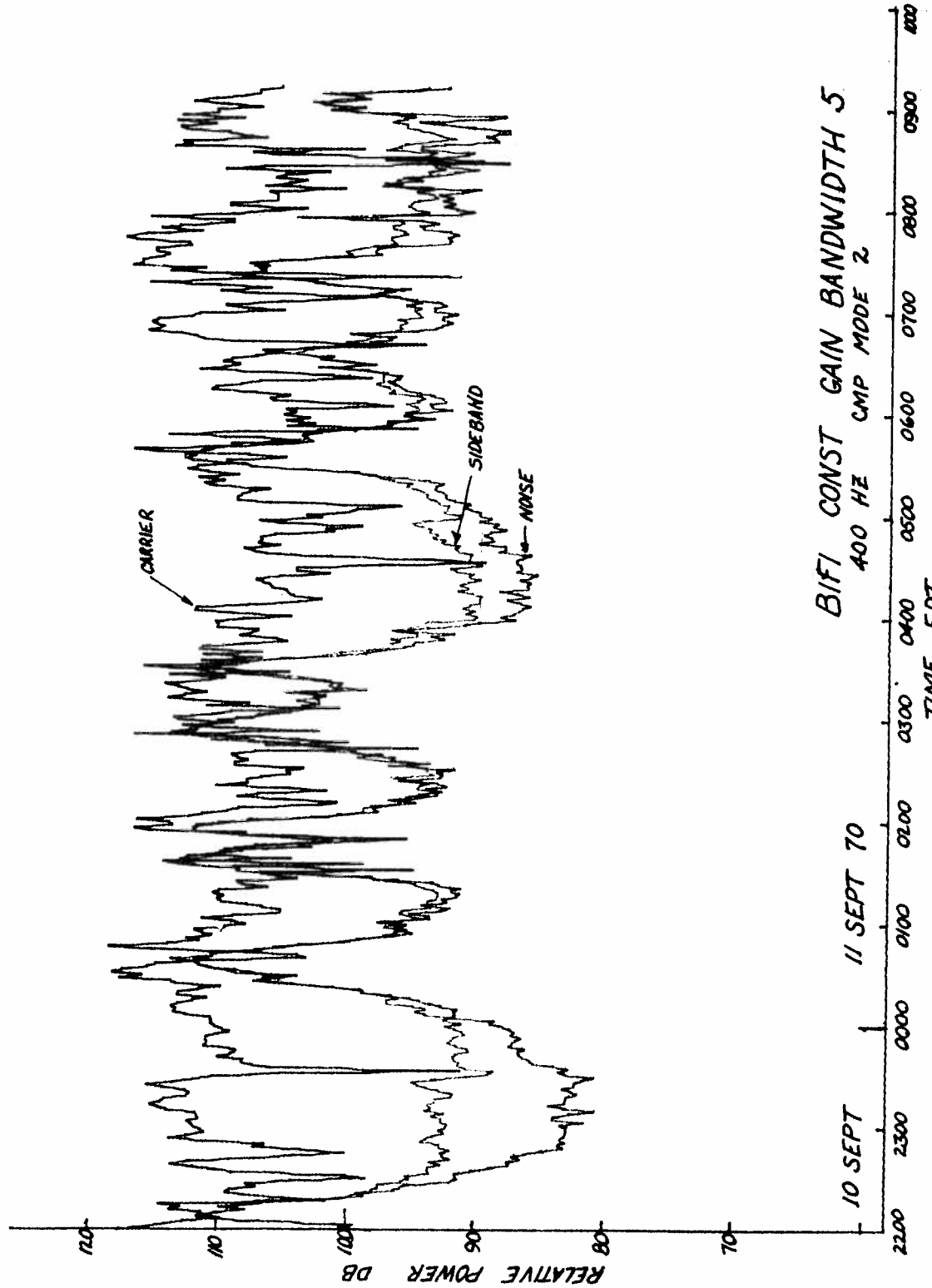

Fig. 12(e). BIFI const. gain-bandwidth 5

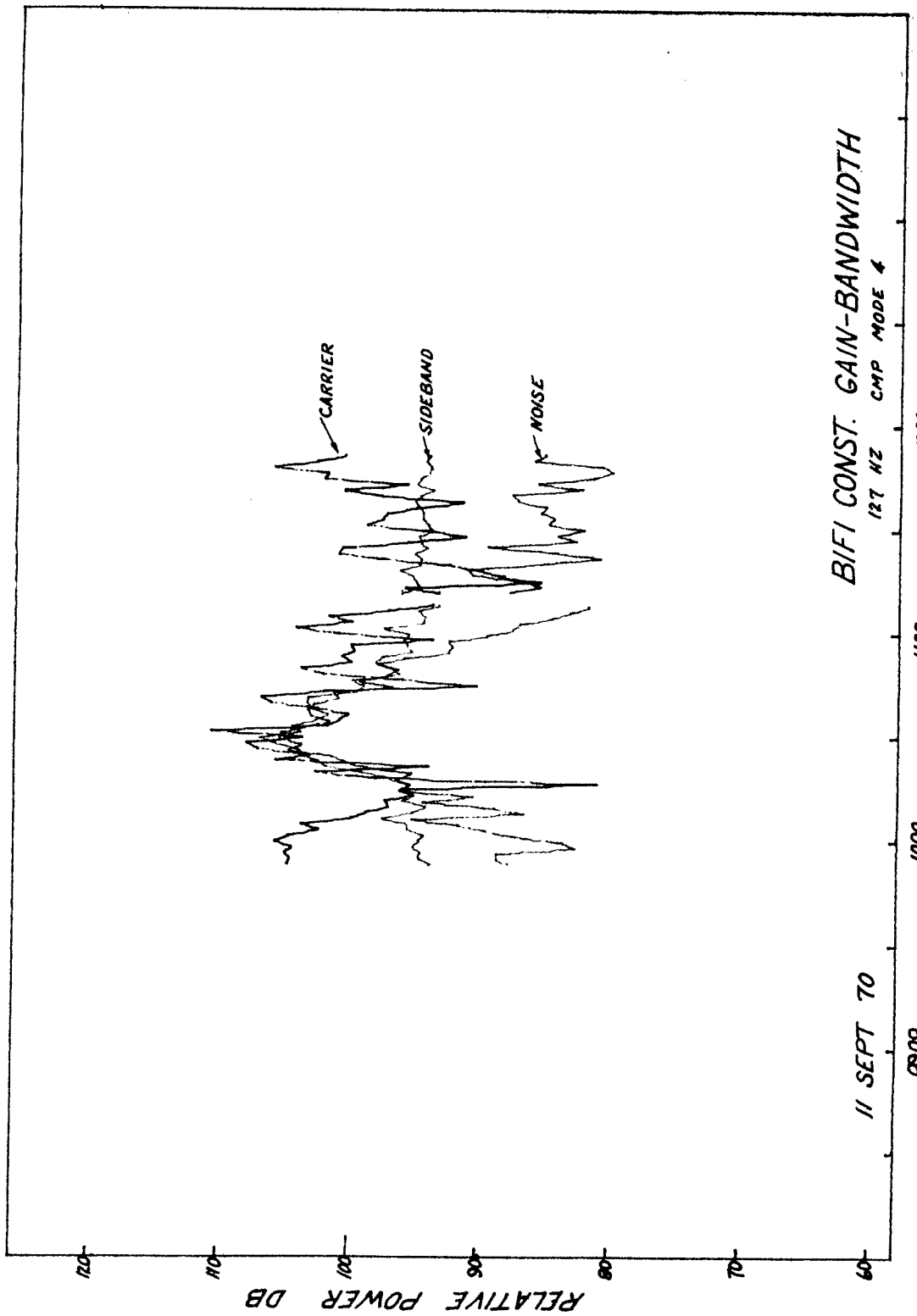

Fig. 13. Constant gain plot for the 127 Hz signal

The last quantity measured in this group of measurements is the carrier phase angle. The carrier phase is plotted in cycles (relative to the phase of the reference oscillator) against time for the 400 Hz transmission in Figs. 14a - 14e and the 127 Hz transmissions in Fig. 15.

The feature that is most important in these plots is the stability of the carrier phase. A "rapid" change of the order of one cycle per hour at 400 Hz (such as 0330 - 0530 on 9 September 1970) indicates a stability of 1 part in 1.44×10^6, or a frequency shift of .00028 Hz. Thus for signal processing of CW the BIFI area is very similar to the Straits of Florida.

The excellent stability lends great credulity to the very small fluctuations that do occur. Both the major maxima and major minima are separated by approximately 12 hours, indicating a probable tidal cause. This cyclic behavior is more apparent in Fig. 14f in which carrier angle is plotted against a compressed time scale.

The significant parts of the sideband power measurements for the Cooley-BIFI experiment are summarized in Figs. 16 and 17. Figure 16 consists of an S - N plot of those portions of the data for which S - N exceeded 6 dB for extended periods of time. Figure 17 consists of the unity-gain plot of the same data.

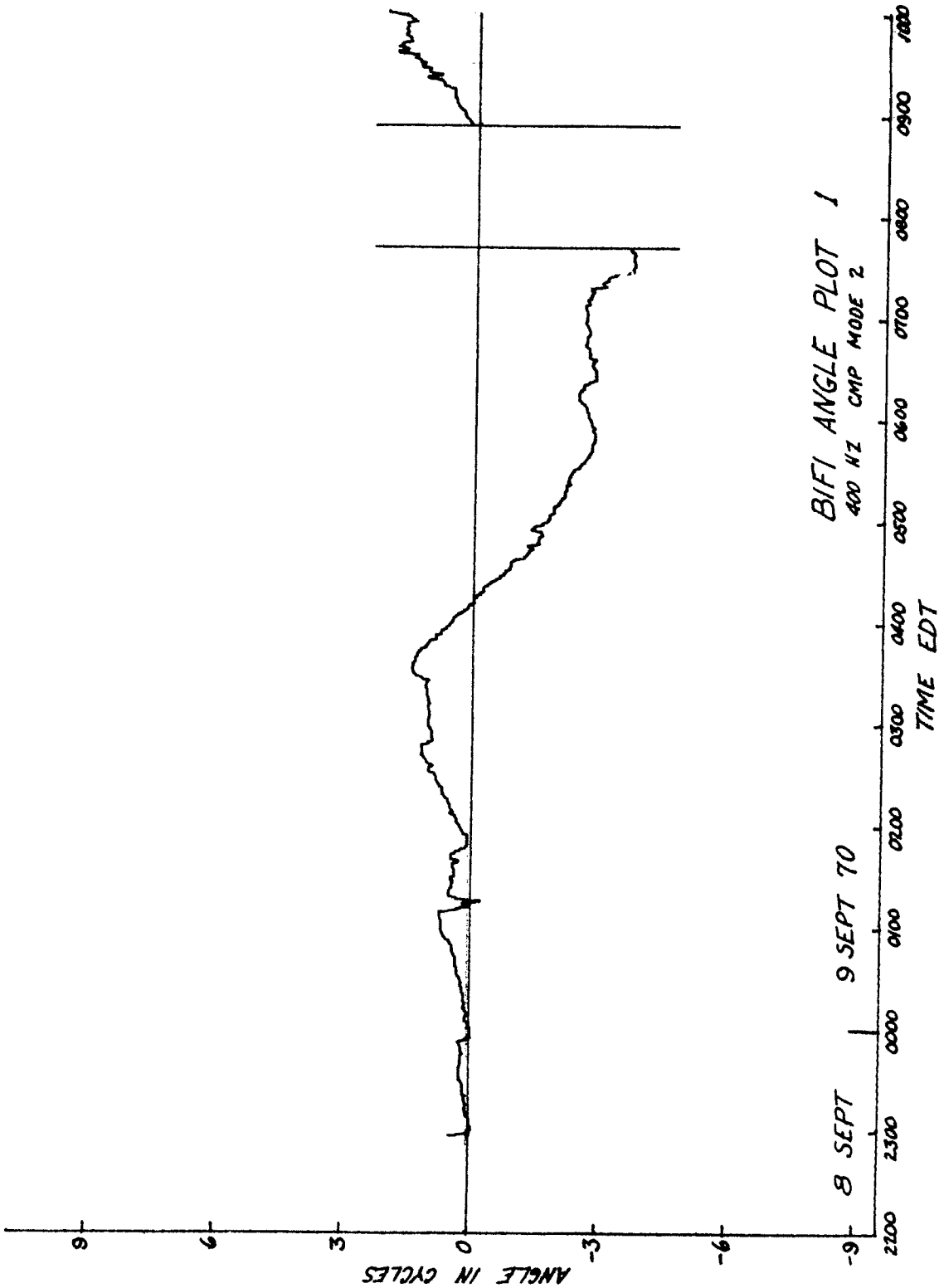

Fig. 14. Angle plot for 400 Hz signal
(a) BIFI angle plot 1

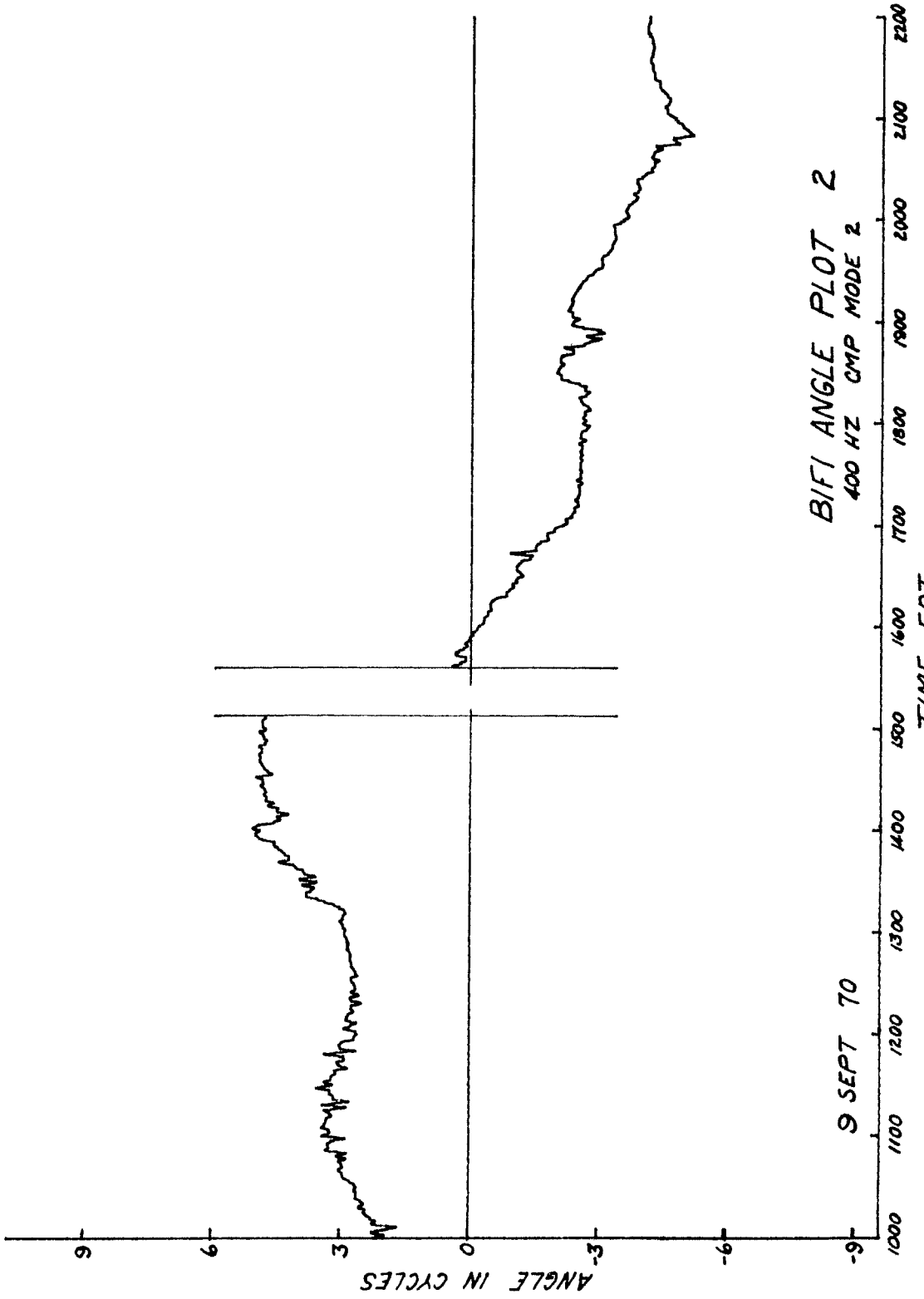

Fig. 14(b). BIFI angle plot 2

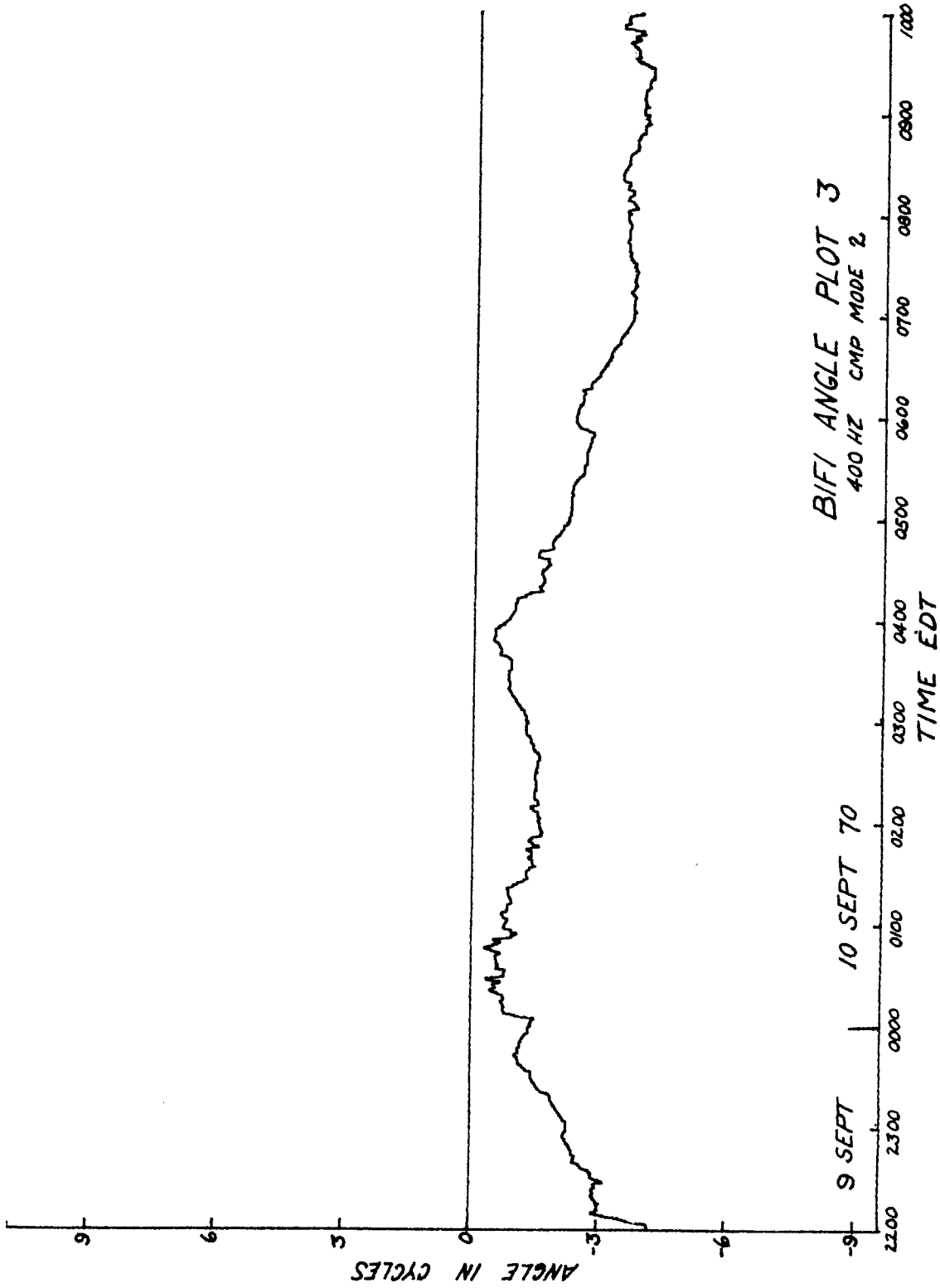

Fig. 14(c) BIFI angle plot 3

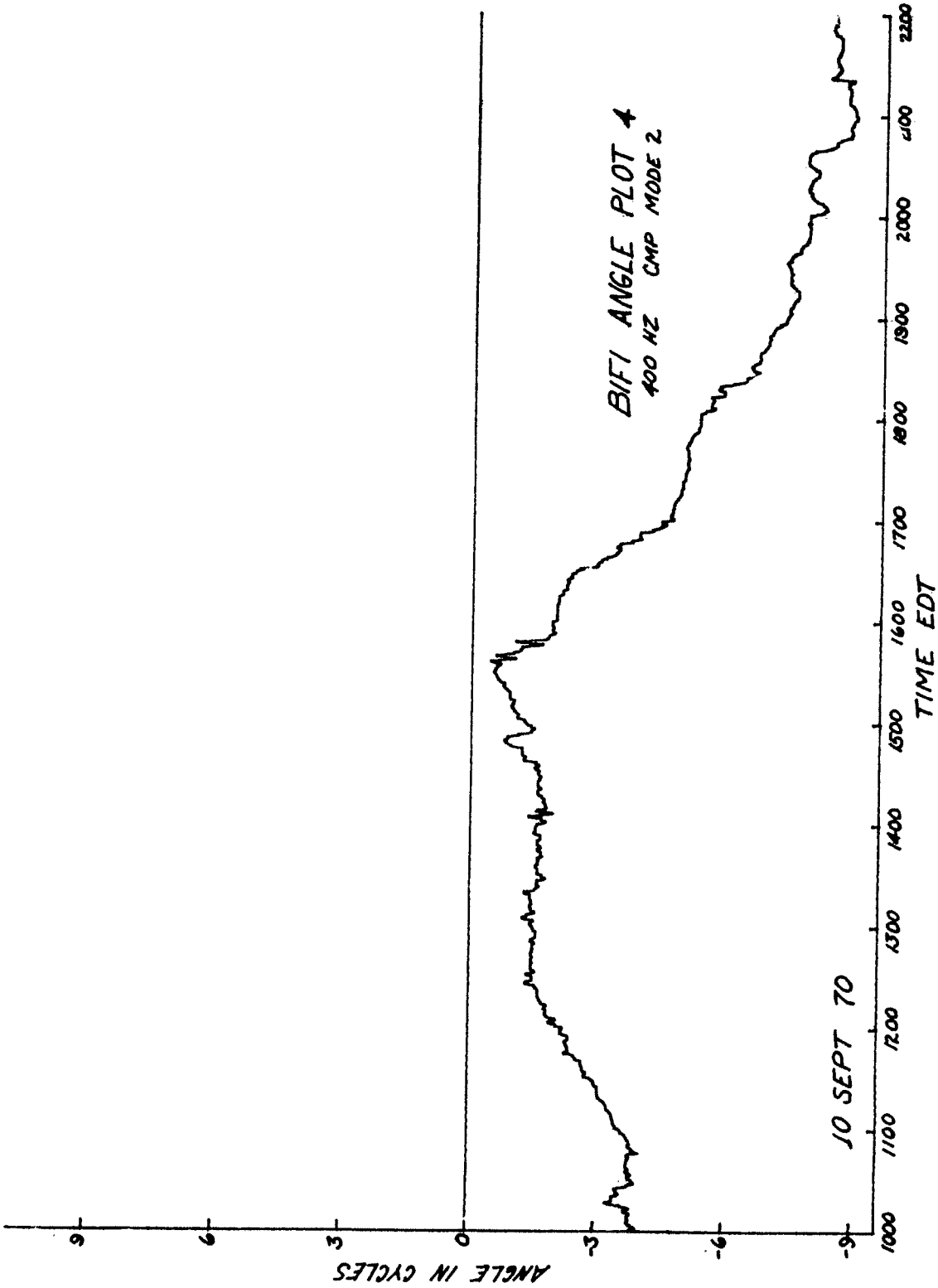

Fig. 14(d). BIFI angle plot 4

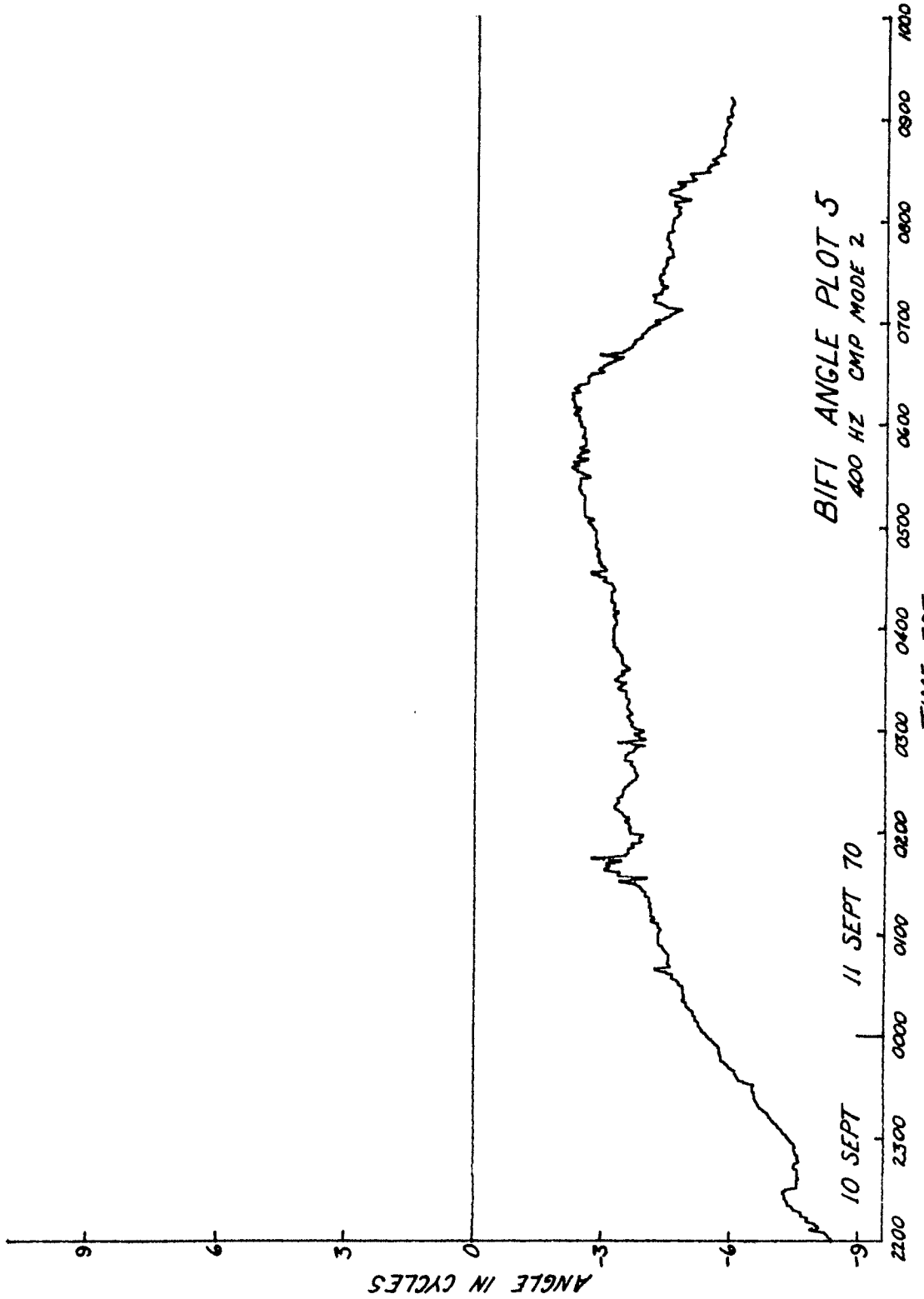

Fig. 14(e). BIFI angle plot 5

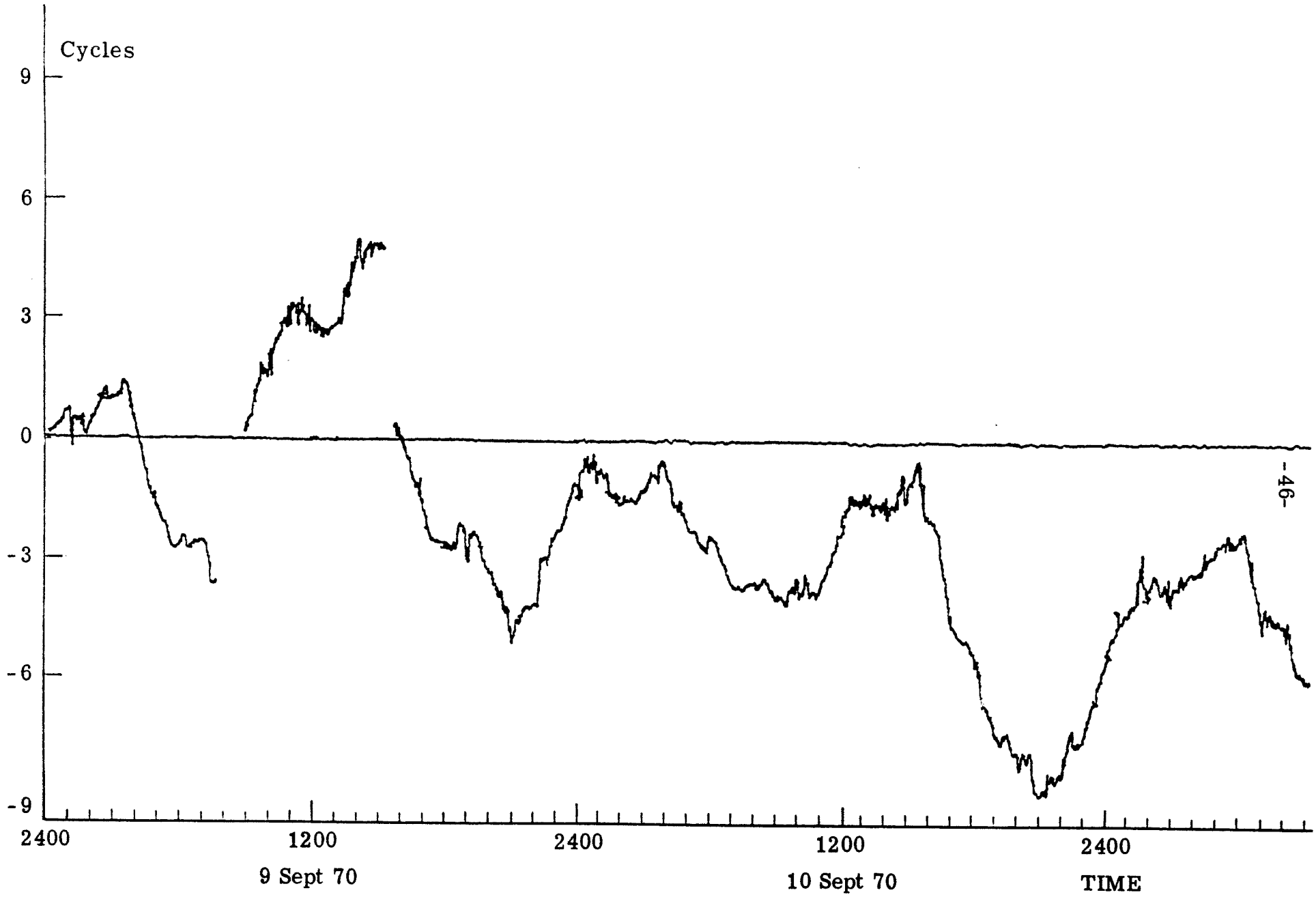

Fig. 14(f). Angle summary plot, 400 Hz

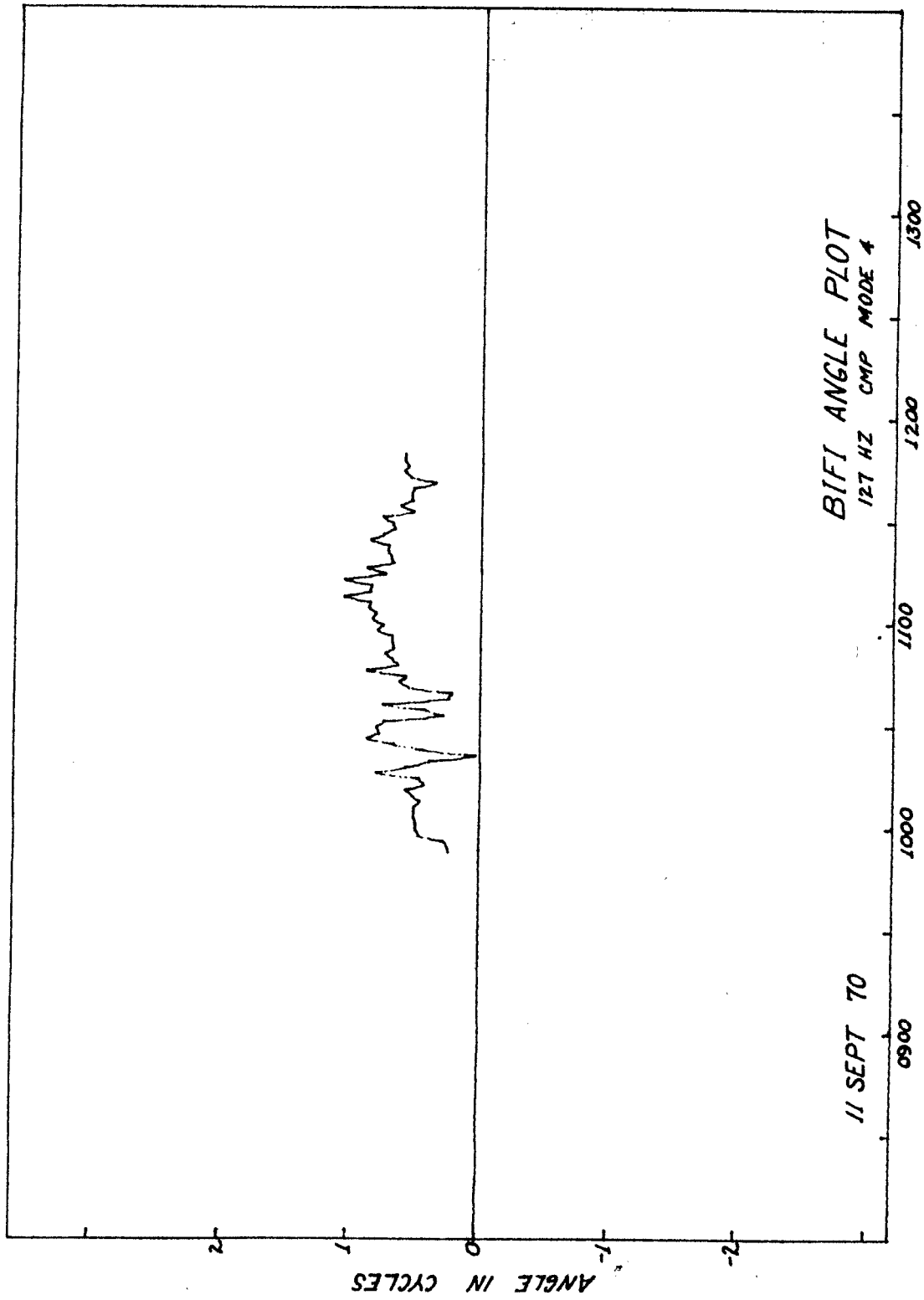

Fig. 15. Angle plot for 127 Hz signal

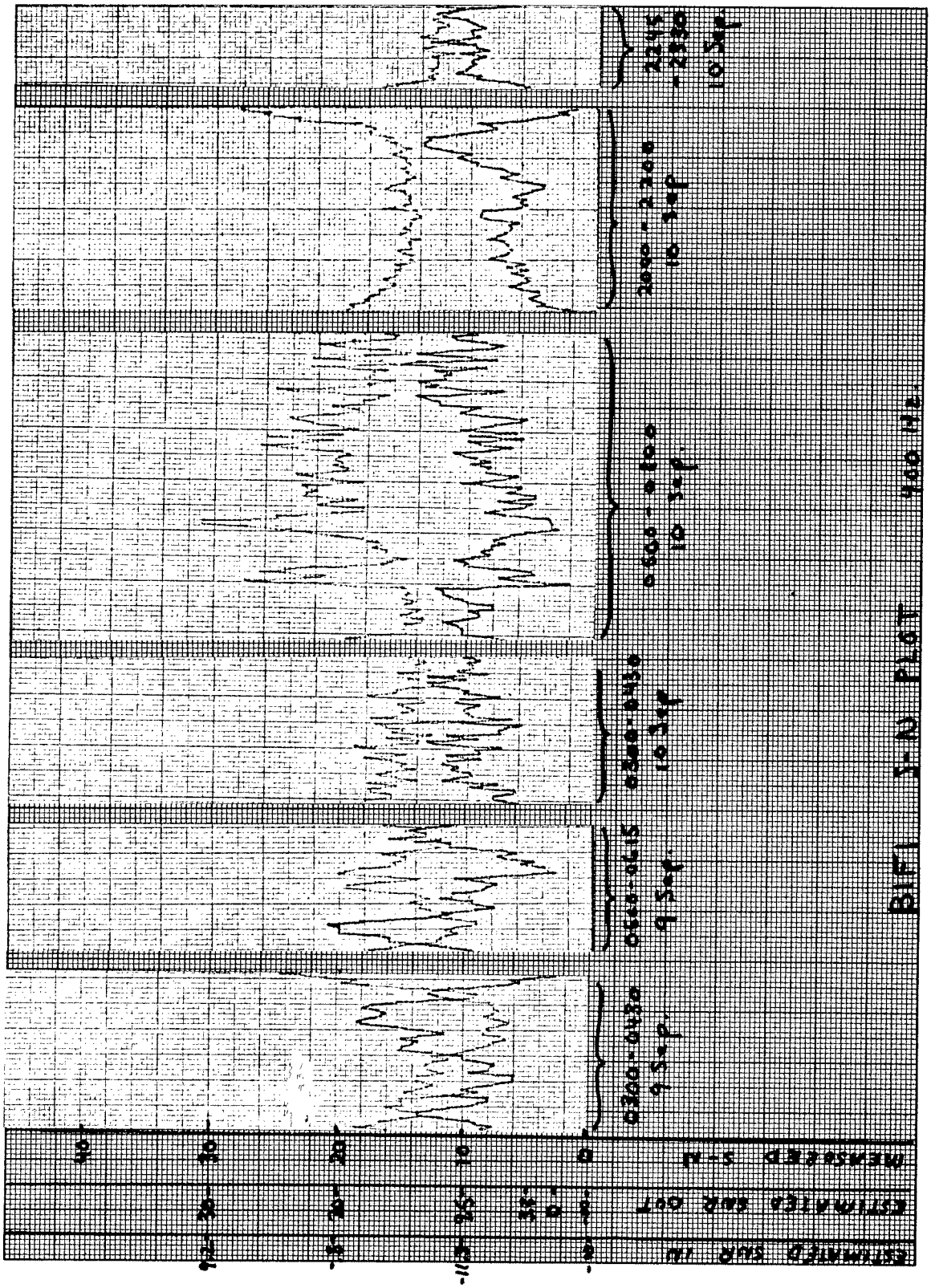

Fig. 16. Sideband signal-to-noise summary plot

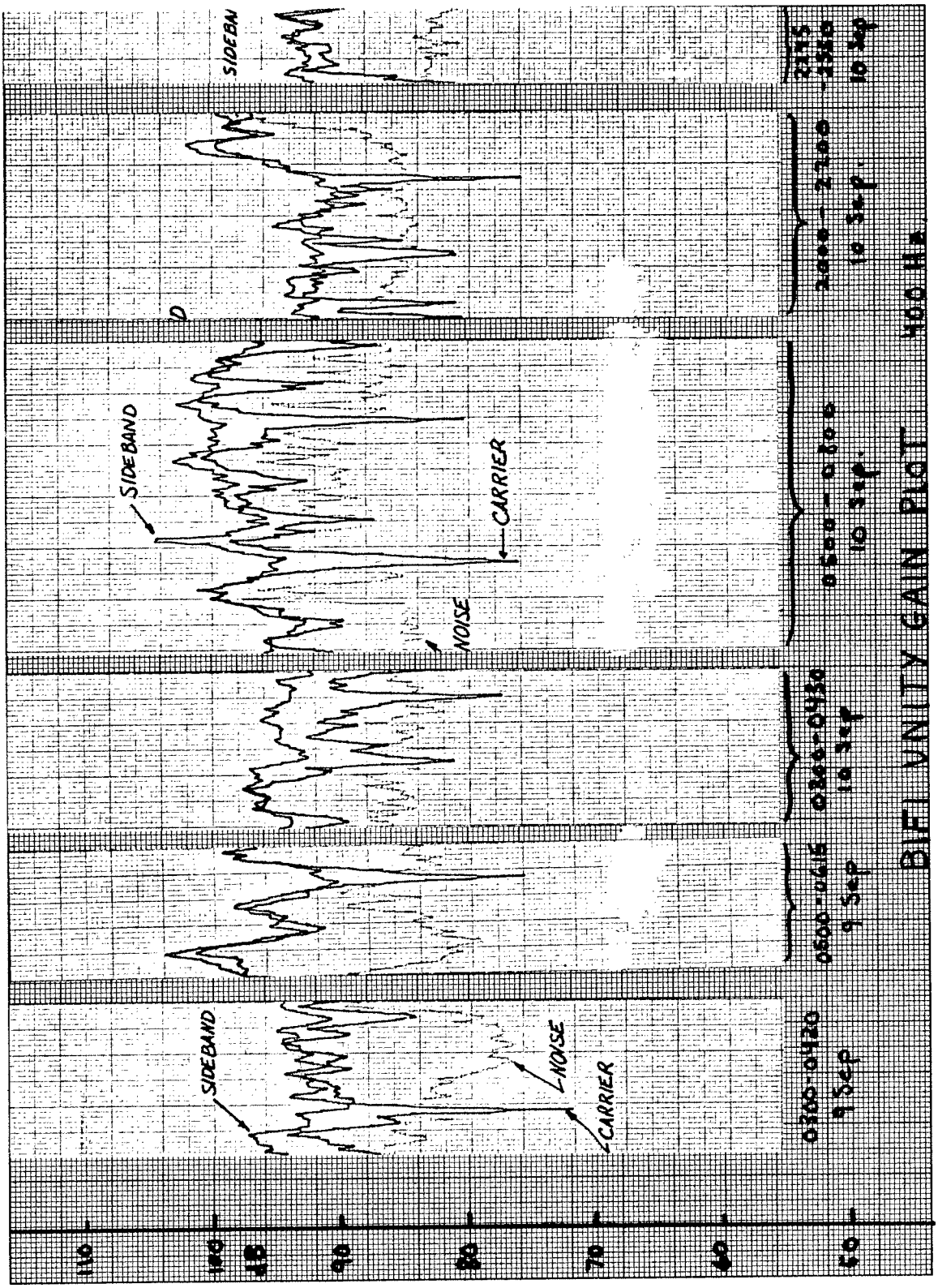

Fig. 17. Unity-gain summary plot

A final note: during the 127 Hz transmission, the level of the received signal was decreased approximately 20 dB at about 1058 on 11 September. This attenuation has been compensated for on all of the power plots by adding in a 20 dB gain after 1058 of 11 September.

II.2 The Surface Reverberation Measurements

The on-line analysis does not indicate a significant surface reverberation effect. The reverb power measurements appear to consist only of the normal amount of noise in the reverb bandwidth as do the reverb spectra displays.

It should be mentioned that the lack of significant reverberation effect measurement might be attributed to the exceptionally calm sea that prevailed during the course of the experiment.

II.3 Multipath Arrival Measurements

The multipath measurement consists of the multipath pictures and the correlation coefficient. Figures 18, 19 and 20 illustrate three sequences of multipath pictures taken at different times during the course of the experiment. Each picture is the envelope of the pulse compression filter output (the magnitude of the cross-correlation between the demodulated received signal and the pulse-compression reference, see Section I.4.3). Successive pictures in each sequence were taken 100 seconds apart. The time axis for each picture is indicated by tick marks. These tick marks are separated by a time equal

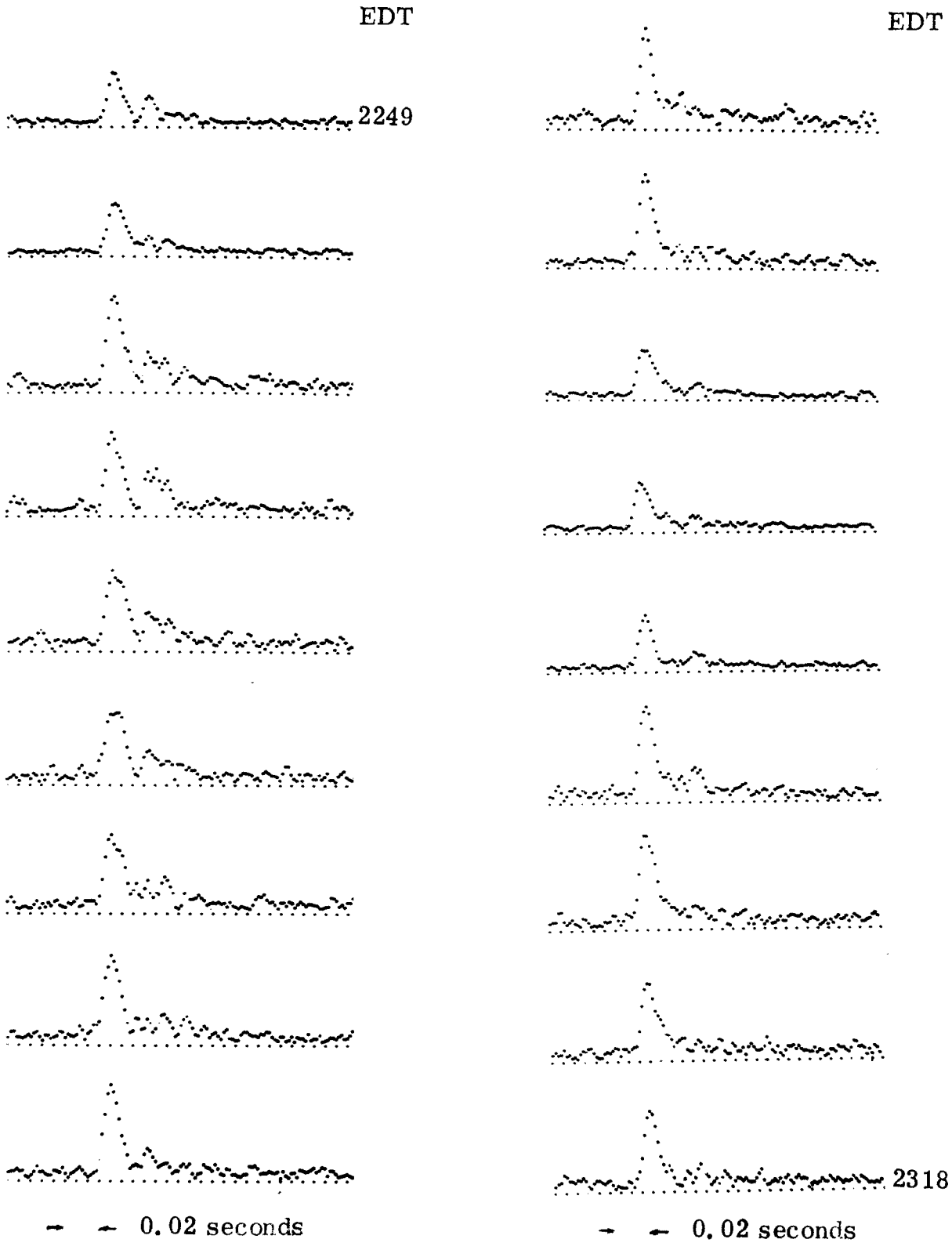

Fig. 18. Successive multipath pictures taken 100 seconds apart between 2249 and 2318 on 10 September 1970 using the 400 Hz signal transmission

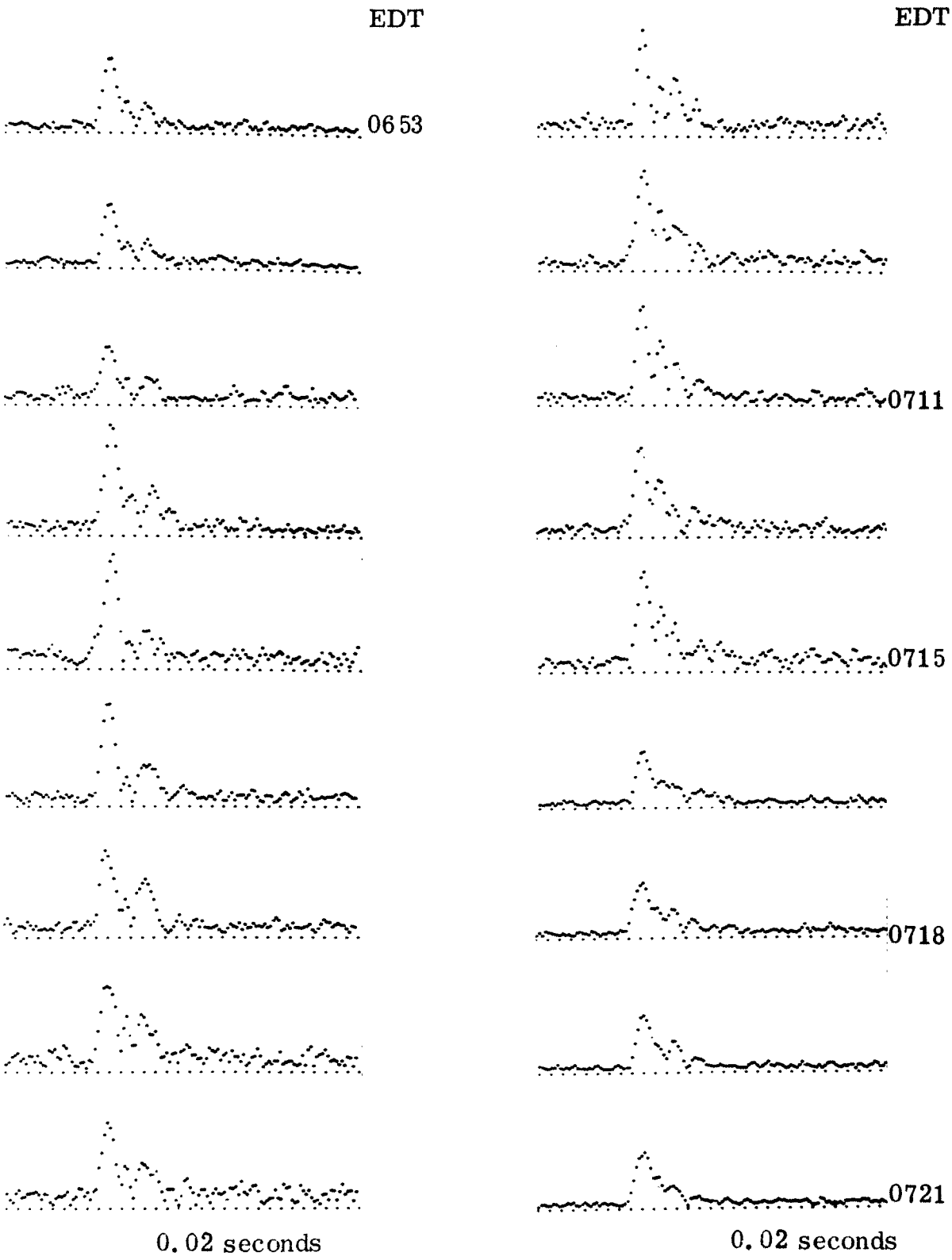

Fig. 19. Successive multipath pictures taken 100 seconds apart between 0653 and 0721 on 10 September 1970 using the 400 Hz signal transmission

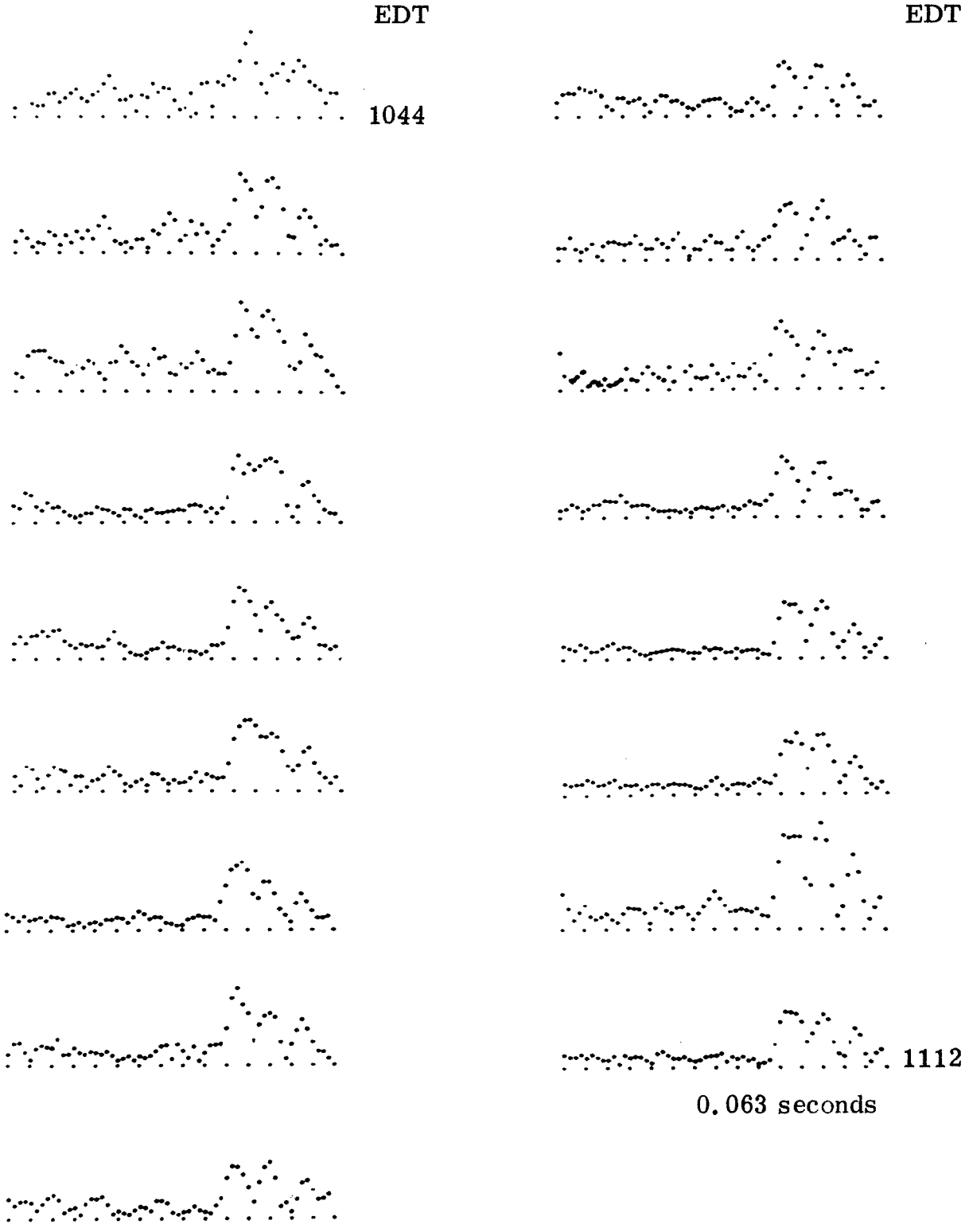

Fig. 20. Successive multipath pictures taken 100 seconds apart between 1044 and 1112 on 11 September 1970 using the 127 Hz signal transmission

to the digit duration in the modulating waveform. Figures 18 and 19 were taken during the 400 Hz transmission so that the time between tick marks is 0.02 seconds. Figure 20 was taken during the 127 Hz transmission so that tick marks are separated by 0.063 seconds. The vertical scaling in the multipath pictures is not the same for each picture but may differ by a factor of a power of two from picture to picture. Thus, it is not necessarily true that an arrival peak in one multipath picture is greater than the corresponding arrival peak in another picture.

The multipath pictures in Fig. 18 were taken between 2249 and 2318 on 10 September 1970. As can be seen from Figs. 8e and 12e, both the sideband signal-to-noise ratio and the C power were large and relatively stable during this period. The multipath pictures in Fig. 19 were taken twelve hours earlier between 0653 and 0721 on 10 September 1970. By referring to Figs. 8c and 12c, it is seen that again both the sideband signal-to-noise ratio and C power are relatively large. In this case, however, the C power suffers a deep fade between 0711 and 0718 with the lowest value of C power occurring at 0715. It appears from Fig. 17 that the correspondence of this deep carrier fade on the multipath pictures is, at most, a slight instability. Detailed investigation of the multipath phase structure is called for.

The multipath pictures in Fig. 20 were taken between 1044

and 1112 on 11 September 1970 during the 127 Hz signal transmission. The temporal spacing between the tick marks is about three times as great as for the 400 Hz transmission, that is the resolution for the 127 Hz transmission is about one-third that for the 400 Hz transmission. At the 127 Hz frequency, at least two and sometimes three strong arrival paths appear, each arrival being separated by about .09 seconds.

The multipath correlation coefficient for delay τ = 100 sec is plotted in decibels against time in Fig. 21 between 2300 and 0500 on the 10th and 11th of September.

The poor signal-to-noise ratio at the processor output during most of this period precluded any attempt to study multipath behavior vs. time.

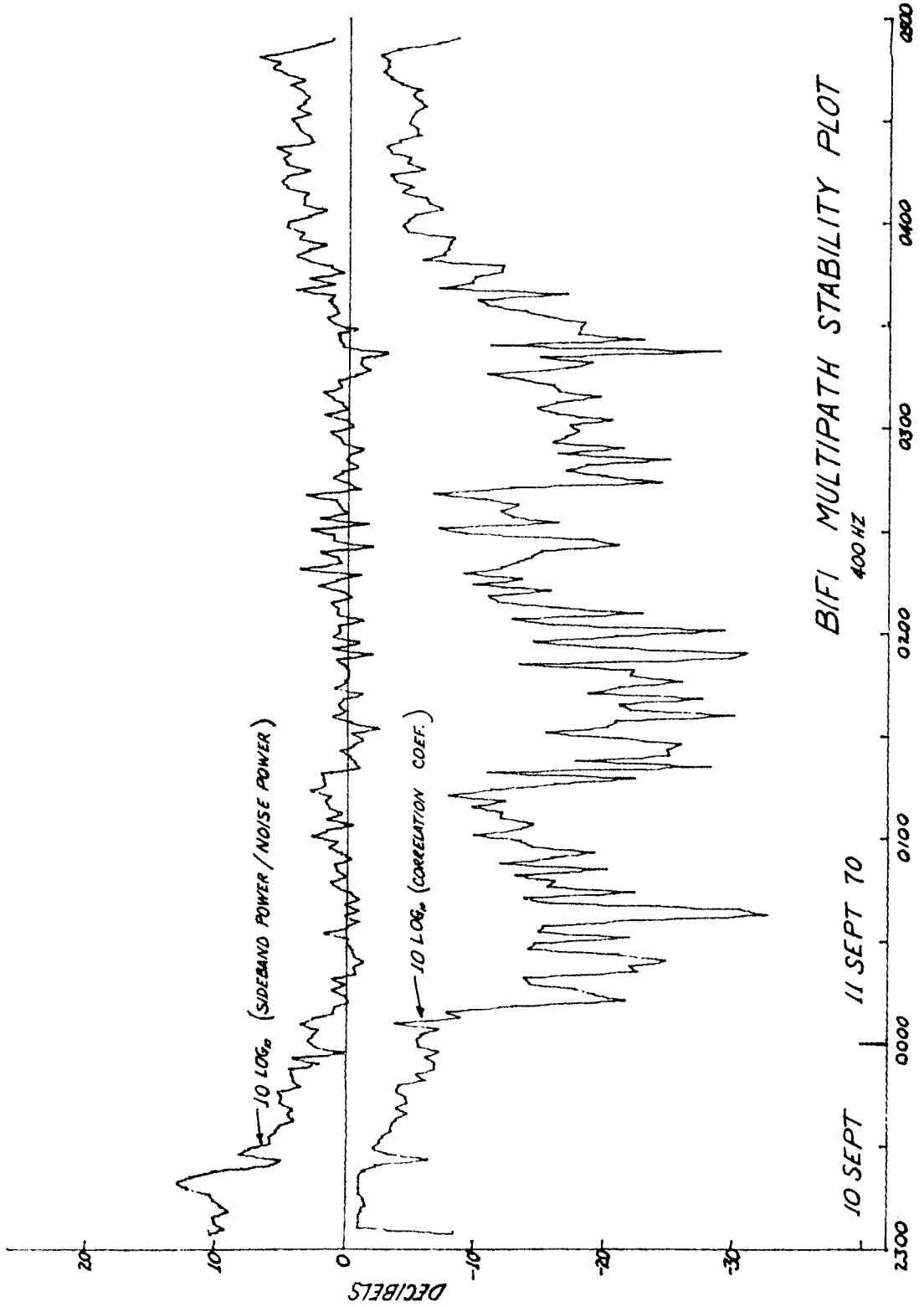

Fig. 21. BIFI multipath stability plot

REFERENCES

1. R. W. Hasse and W. R. Schumacher, BIFI Shallow Water Program, USL Tech. Memo No. 2211-281-68, December 4, 1968.

2. Frequency Stability of External Frequency Standards to be used in BIFI Experiments by University of Michigan in Sept. 1970, Memo from Hans J. Arens, to Code 2211, dated 21 September 1970.

DISTRIBUTION LIST

	No. of Copies
Office of Naval Research (Code 468) (Code 102-OS) (Code 480) Navy Department Washington, D. C. 20360	1 1 1
Director, Naval Research Laboratory Technical Information Division Washington, D. C. 20390	6
Director Office of Naval Research Branch Office 1030 East Green Street Pasadena, California 91101	1
Office of Naval Research San Francisco Area Office 1076 Mission Street San Francisco, California 94103	1
Director Office of Naval Research Branch Office 495 Summer Street Boston, Massachusetts 02210	1
Office of Naval Research New York Area Office 207 West 24th Street New York, New York 10011	1
Director Office of Naval Research Branch Office 536 S. Clark Street Chicago, Illinois 60605	1
Director Naval Research Laboratory Attn: Library, Code 2029 (ONRL) Washington, D. C. 20390	8

DISTRIBUTION LIST (Cont.)

	No. of Copies
Commander Naval Ordnance Laboratory Acoustics Division White Oak, Silver Spring, Maryland 20907 Attn: Dr. Zaka Slawsky	1
Commanding Officer Naval Ship Research & Development Center Annapolis, Maryland 21401	1
Commander Naval Undersea Research & Development Center San Diego, California 92132 Attn: Dr. Dan Andrews Mr. Henry Aurand	2
Chief Scientist Navy Underwater Sound Reference Division P. O. Box 8337 Orlando, Florida 32800	1
Commanding Officer and Director Navy Underwater Systems Center Fort Trumbull New London, Connecticut 06321	1
Commander Naval Air Development Center Johnsville, Warminster, Pennsylvania 18974	1
Commanding Officer and Director Naval Ship Research and Development Center Washington, D. C. 20007	1
Superintendent Naval Postgraduate School Monterey, California 93940	1
Commanding Officer & Director Naval Ship Research & Development Center* Panama City, Florida 32402	1

*Formerly Mine Defense Lab.

DISTRIBUTION LIST (Cont.)

	No. of Copies
Naval Underwater Weapons Research & Engineering Station Newport, Rhode Island 02840	1
Superintendent Naval Academy Annapolis, Maryland 21401	1
Scientific and Technical Information Center 4301 Suitland Road Washington, D. C. 20390 Attn: Dr. T. Williams Mr. E. Bissett	2
Commander Naval Ordnance Systems Command Code ORD-03C Navy Department Washington, D. C. 20360	1
Commander Naval Ship Systems Command Code SHIPS 037 Navy Department Washington, D. C. 20360	1
Commander Naval Ship Systems Command Code SHIPS 00V1 Washington, D. C. 20360 Attn: CDR Bruce Gilchrist Mr. Carey D. Smith	2
Commander Naval Undersea Research & Development Center 3202 E. Foothill Boulevard Pasadena, California 91107	1
Commanding Officer Fleet Numerical Weather Facility Monterey, California 93940	1

DISTRIBUTION LIST (Cont.)

	No. of Copies
Defense Documentation Center Cameron Station Alexandria, Virginia 22314	20
Dr. James Probus Office of the Assistant Secretary of the Navy (R&D) Room 4E741, The Pentagon Washington, D. C. 20350	1
Mr. Allan D. Simon Office of the Secretary of Defense DDR&E Room 3E1040, The Pentagon Washington, D. C. 20301	1
CAPT J. Kelly Naval Electronics Systems Command Code EPO-3 Washington, D. C. 20360	1
Chief of Naval Operations Room 5B718, The Pentagon Washington, D. C. 20350 Attn: Mr. Benjamin Rosenberg	1
Chief of Naval Operations Rm 4C559, The Pentagon Washington, D. C. 20350 Attn: DCR J. M. Van Metre	1
Chief of Naval Operations 801 No. Randolph St. Arlington, Virginia 22203	1
Dr. Melvin J. Jacobson Rensselaer Polytechnic Institute Troy, New York 12181	1
Dr. Charles Stutt General Electric Co. P. O. Box 1088 Schenectady, New York 12301	1

DISTRIBUTION LIST (Cont.)

	No. of Copies
Dr. Alan Winder EDO Corporation College Point, New York 11356	1
Dr. T. G. Birdsall Cooley Electronics Lab. University of Michigan Ann Arbor, Michigan 48105	1
Dr. John Steinberg University of Miami Institute of Marine & Atmospheric Sciences Miami, Florida 33149	1
Mr. Robert Cunningham Bendix Corporation 11600 Sherman Way North Hollywood, California 91606	1
Dr. H. S. Hayre University of Houston Cullen Boulevard Houston, Texas 77004	1
Dr. Robert R. Brockhurst Woods Hole Oceanographic Institute Woods Hole, Massachusetts 02543	1
Dr. Stephen Wolff Johns Hopkins University Baltimore, Maryland 21218	1
Dr. M. A. Basin Litton Industries 8000 Woodley Avenue Van Nuys, California 91409	1
Dr. Albert Nuttall Navy Underwater Systems Center Fort Trumbull New London, Connecticut 06320	1

DISTRIBUTION LIST (Cont.)

	No. of Copies
Dr. Philip Stocklin Raytheon Company P. O. Box 360 Newport, Rhode Island 02841	1
Dr. H. W. Marsh Navy Underwater Systems Center Fort Trumbull New London, Connecticut 06320	1
Dr. David Middleton 35 Concord Ave., Apt. #1 Cambridge, Massachusetts 02138	1
Mr. Richard Vesper Perkin-Elmer Corporation Electro-Optical Division Norwald, Connecticut 06852	1
Dr. Donald W. Tufts University of Rhode Island Kingston, Rhode Island 02881	1
Dr. Loren W. Nolte Dept. of Electrical Engineering Duke University Durham, North Carolina 27706	1
Dr. Thomas W. Ellis Texas Instruments, Inc. 13500 North Central Expressway Dallas, Texas 75231	1
Mr. Robert Swarts Honewell, Inc., Marine Systems Center 5303 Shilshole Ave., N. W. Seattle, Washington, 98107	1
Mr. Charles Loda Institute for Defense Analyses 400 Army-Navy Drive Arlington, Virginia 22202	1

DISTRIBUTION LIST (Cont.)

	No. of Copies
Mr. Beaumont Buck General Motors Corporation Defense Research Division 6767 Holister Ave. Goleta, California 93017	1
Dr. M. Weinstein Underwater Systems, Inc. 8121 Georgia Avenue Silver Spring, Maryland 20910	1
Dr. Harold Saxton 1601 Research Blvd. TRACOR, Inc. Rockville, Maryland 20850	1
Dr. Thomas G. Kincaid General Electric Company P. O. Box 1088 Schenectady, New York 12305	1
Applied Research Laboratories The University of Texas at Austin Austin, Texas 78712 Attn: Dr. Loyd Hampton Dr. Charles Wood	3
Dr. Paul McElroy Woods Hole Oceanographic Institution Woods Hole, Massachusetts 02543	1
Dr. John Bouyoucos General Dynamics/ Electronics 1400 N. Goodman Street, P. O. Box 226 Rochester, New York 14603	1
Hydrospace Research Corporation 5541 Nicholson Lane Rockville, Maryland 20852 Attn: CDR Craig Olson	1
Cooley Electronics Laboratory University of Michigan Ann Arbor, Michigan 48105	25